Journal of Computational Electronics (2025) 24:151
https://doi.org/10.1007/s10825-025-02389-0

A current–voltage model for organic solar cells with carrier transport layers based on a combined analytical and regression approach

M. L. Inche Ibrahim[1]

Received: 4 December 2024 / Accepted: 7 July 2025 / Published online: 31 July 2025

Abstract
Organic solar cells (OSCs) have many potential applications due to attributes such as high mechanical flexibility, relatively low production cost, good transparency, and lightweight. Since the power conversion efficiency (PCE) of OSCs is relatively low currently, their PCE must be further improved to better exploit their potential in the future. The use of carrier transport layers (CTLs) is essential to maximize the PCE of OSCs. Therefore, a model that can accurately and reliably describe the current voltage (J-V) characteristics of OSCs with CTLs is also essential. Such a model is proposed in this paper. The proposed model is based on the semiconductor drift–diffusion transport model, which is the standard physics-based approach for modeling semiconductor devices including solar cells. In obtaining the proposed model, the approximate electric fields and the approximate boundary conditions in OSCs with CTLs are derived and then applied to the carrier continuity equations, which are then solved using a recently proposed combined analytical and regression method. The use of the recently proposed method makes the proposed model to be more accurate than analytical drift–diffusion-based J-V models and more reliable than numerical drift–diffusion-based J-V models. We verify that the proposed model works well and show that it can provide insights into how to optimize the design and improve the PCE of OSCs with CTLs. Therefore, owing to its unique quality, the proposed model can be a valuable tool for predicting and analyzing the J-V characteristics, and ultimately for improving the design and the PCE of OSCs with CTLs.

Keywords Blocking layer · Device physics · Metal oxides · Organic semiconductors · Photovoltaic cells · Semiconductor device modeling

1 Introduction

Organic solar cells (OSCs) have many potential applications due to attributes such as high mechanical flexibility, relatively low production cost, good transparency, and lightweight [1–5]. For example, OSCs are ideal candidates as power sources for low-power indoor devices (e.g., devices for the Internet of Things [4]) and for the next generation biomedical devices [5]. However, there are hurdles that need to be overcome before OSCs can be fully exploited and commercialized. Two main hurdles for OSCs are their relatively poor efficiency [6] and performance degradation, particularly under harsh operating conditions [1].

✉ M. L. Inche Ibrahim
mlukmanibrahim@gmail.com; lukmanibrahim@iium.edu.my

[1] Department of Science in Engineering, Faculty of Engineering, International Islamic University Malaysia, Kuala Lumpur, Malaysia

A well-known way to improve the power conversion efficiency (PCE) of OSCs is to incorporate a hole transport layer (HTL) between the active layer and the anode, and an electron transport layer (ETL) between the active layer and the cathode [7]. An HTL must be able to efficiently extract holes from the active layer to the anode and block the extractions of electrons and excitons from the active layer to the anode [7]. Similarly, an ETL must be able to efficiently extract electrons from the active layer to the cathode and block the extractions of holes and excitons from the active layer to the cathode [7]. Since the use of these carrier transport layers (CTLs), i.e., HTL and ETL, is vital in maximizing the PCE of OSCs [7], a model that can accurately and reliably describe the current–voltage (J-V) characteristics of OSCs with CTLs is needed to better understand and predict, and ultimately to further enhance the performance of OSCs.

The semiconductor drift–diffusion model is regarded as the standard physics-based approach for modeling semiconductor devices including solar cells. Recently, a

drift–diffusion based J-V model for OSCs was proposed where a combined analytical and regression method was used in deriving the model [8]. It was shown that the use of the method in Ref. [8] makes the resulting drift–diffusion-based J-V model in Ref. [8] to be more accurate than analytical drift–diffusion-based J-V models (because the model in Ref. [8] allows us to consider realistic carrier generation profiles and recombination mechanisms, which cannot be considered in purely analytical J-V models) and more reliable than numerical drift–diffusion-based J-V models (such as models based on the finite difference method) [8]. However, the J-V model proposed in Ref. [8] is based on the basic OSC structure without CTLs. The motivation of this paper is to create a J-V model for OSCs that is more accurate than analytical drift–diffusion-based J-V models and more reliable than numerical drift–diffusion-based J-V models, like the J-V model proposed in Ref. [8], but with the inclusion of the all-important CTLs. To achieve the objective of this paper, we derive the approximate electric fields and the approximate boundary conditions in OSCs with CTLs, which are then applied to the carrier continuity equations, which are then solved using the method proposed in Ref. [8] in order to obtain the J-V model. As mentioned earlier, the use of the method proposed in Ref. [8] makes the J-V model proposed in this paper to be more accurate than analytical drift–diffusion-based J-V models and more reliable than numerical drift–diffusion-based J-V models, and hence, the model proposed in this paper can be a valuable tool for understanding the operation, improving the PCE, and optimizing the design (to reduce the cost for example) of OSCs with CTLs.

2 Model for OSCs with CTLs

In this section, we present a new J-V model for OSCs with CTLs. Section 2.1 describes the working operation and basic equations for OSCs. In Sect. 2.2, we derive the approximate electric fields inside the HTL, active layer, and ETL for various device settings. In Sect. 2.3, we derive the approximate boundary conditions for OSCs with and without CTLs. Finally, in Sect. 2.4, we describe how the carrier recombination rates are calculated, and then how the current densities are calculated in order to obtain the J-V characteristics.

2.1 Working principle and basic equations

Figure 1 illustrates the device structures and the energy levels for an OSC without and with CTLs, while Table 1 shows a list of mathematical symbols used in this paper. The organic active layer is made of a blend of an electron donating material (called donor) and an electron accepting material (called acceptor), giving rise to what is called the bulk heterojunction structure. When light is absorbed by the active layer, strongly bound electron–hole pairs called excitons are created. When the excitons reach the donor–acceptor interface, they generally transform into charge-transfer (CT) states [9]. A CT state consists of an electron in the acceptor that still binds with a hole in the donor [9]. A CT state may decay to the ground state (which is a geminate recombination) or separate into a free electron and a free hole [9]. Free or mobile electrons (holes) can move inside the acceptor (donor) network and can be collected by the cathode (anode) to generate an electric current. When a free electron and a free hole encounter each other near the donor–acceptor interface, they can undergo what is called nongeminate recombination [9]. There are three possible types of nongeminate recombination: nongeminate bimolecular recombination in which the recombination reproduces CT states [9, 10], trap-assisted (or Shockley–Read–Hall) recombination [9, 10], and Auger recombination (but uncommon in OSCs) [10].

In order for the free holes in the active layer to be efficiently collected by the anode, we need to ensure that there are no hole energy barriers at the active layer-HTL interface and at the HTL-anode interface so that the free holes can easily move from the active layer to the HTL and then from the HTL to the anode. To eliminate the hole energy barriers mentioned above, we need to ensure that $E_{Fa} \geq \mathrm{HOMO_H} \geq \mathrm{HOMO_{dA}}$ (or $E_{Fa} \geq \mathrm{VBM_H} \geq \mathrm{HOMO_{dA}}$ if an inorganic semiconductor is used as the HTL). On the other hand, to ensure that the HTL blocks the free electrons in the active layer from being collected by the anode, there should be a significant electron energy barrier at the active layer-HTL interface so that the free electrons in the active layer are prevented from moving to the HTL, and thus to the anode. To create the electron energy barrier mentioned above, $\mathrm{LUMO_H}$ (or $\mathrm{CBM_H}$ if an inorganic semiconductor is used as the HTL) should be considerably higher than $\mathrm{LUMO_{aA}}$. Similarly, to allow free electrons in the active layer to be efficiently collected by the cathode, we need to ensure that $\mathrm{LUMO_{aA}} \geq \mathrm{LUMO_E} \geq E_{Fc}$ (or $\mathrm{LUMO_{aA}} \geq \mathrm{CBM_E} \geq E_{Fc}$ if an inorganic semiconductor is used as the ETL), whereas $\mathrm{HOMO_E}$ (or $\mathrm{VBM_E}$ if an inorganic semiconductor is used as the ETL) should be considerably lower than $\mathrm{HOMO_{dA}}$ so that the free holes in the active layer are prevented from moving to the ETL, and thus to the cathode. Furthermore, as can be seen later in Sect. 2.2, the better the alignments between E_{Fa}, $\mathrm{HOMO_H}$, and $\mathrm{HOMO_{dA}}$ (or between E_{FH} and $\mathrm{HOMO_{dA}}$ if the HTL is made of a semiconductor that contains mobile carriers) and between E_{Fc}, $\mathrm{LUMO_E}$, and $\mathrm{LUMO_{aA}}$ (or between E_{FE} and $\mathrm{LUMO_{aA}}$ if the ETL is made of a semiconductor that contains mobile carriers, the higher the strength of the electric field inside the device. Since the electric field inside the device is important in transporting the charge carriers, the mentioned energy

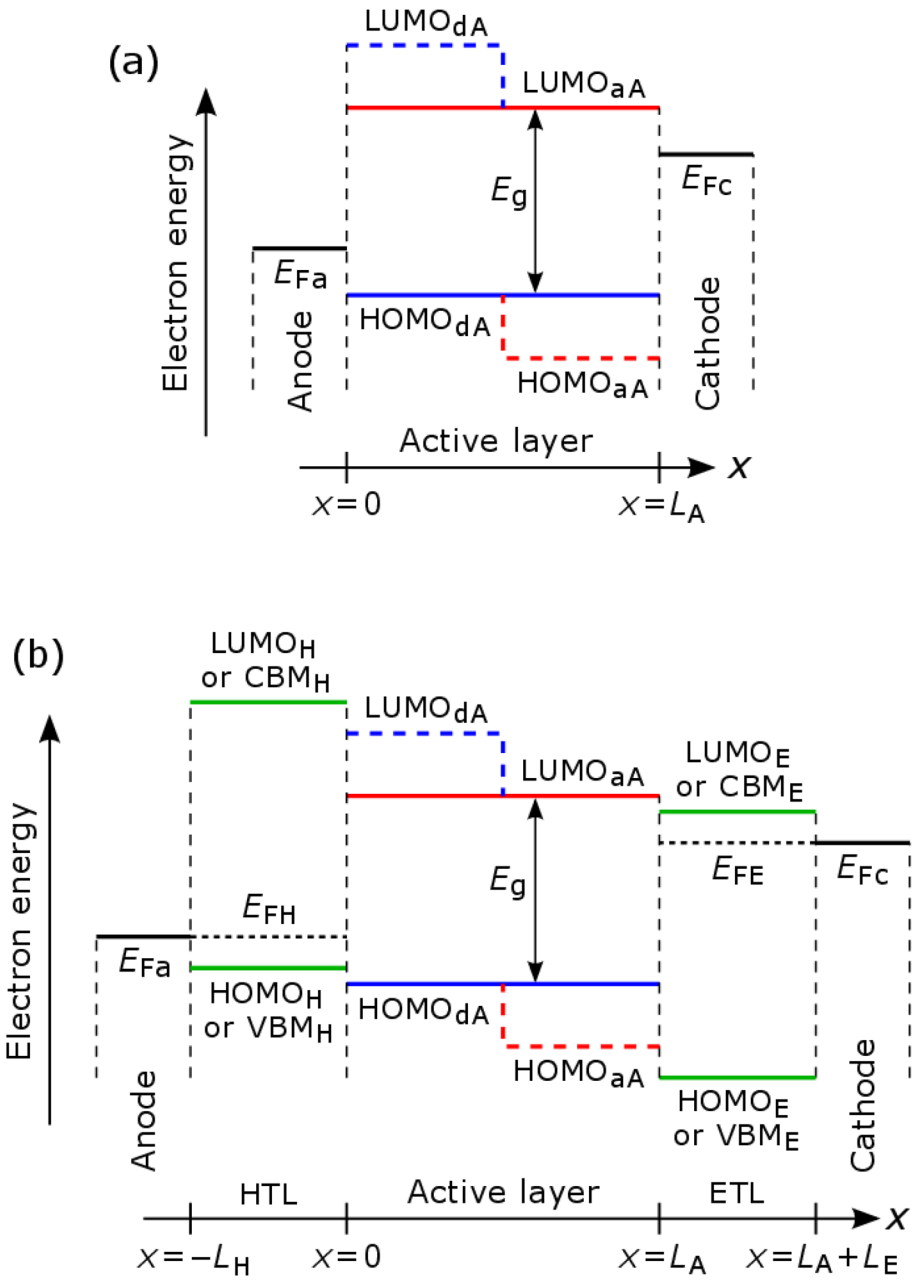

Fig. 1 Schematics illustrating an OSC without CTLs [panel (**a**)] and an OSC with CTLs [panel (**b**)]. $LUMO_H$ denotes the lowest unoccupied molecular orbital (LUMO) of the HTL if the HTL is an organic semiconductor, whereas CBM_H denotes the conduction band minimum (CBM) of the HTL if the HTL is an inorganic semiconductor. $HOMO_H$ denotes the highest occupied molecular orbital (HOMO) of the HTL if the HTL is an organic semiconductor, whereas VBM_H denotes the valence band maximum (VBM) of the HTL if the HTL is an inorganic semiconductor. $LUMO_E$ and $HOMO_E$ denote the LUMO and HOMO of the ETL, respectively, if the ETL is an organic semiconductor. CBM_E and VBM_E denote the CBM and VBM of the ETL, respectively, if the ETL is an inorganic semiconductor. $LUMO_{dA}$ and $HOMO_{dA}$ denote the LUMO and HOMO of the donor of the active layer, respectively. $LUMO_{aA}$ and $HOMO_{aA}$ denote the LUMO and HOMO of the acceptor of the active layer, respectively. E_g denotes the effective band gap, which is the difference between $LUMO_{aA}$ and $HOMO_{dA}$. E_{Fa} and E_{Fc} denote the Fermi levels of the anode and cathode, respectively. E_{FH} and E_{FE} denote the Fermi levels of the HTL and ETL, respectively, which are especially important if the HTL and ETL are made of semiconductors that contain mobile carriers. L_A, L_H, and L_E denote the thicknesses of the active layer, HTL, and ETL, respectively. The edges of the active layer are fixed at $x = 0$ and $x = L_A$ as shown in the figure

Table 1 List of symbols

Symbol	Description
x	Position in OSC in one dimensional coordinate system
$\mathrm{LUMO_H}$	Lowest unoccupied molecular orbital (LUMO) of the HTL
$\mathrm{CBM_H}$	Conduction band minimum (CBM) of the HTL
$\mathrm{HOMO_H}$	Highest occupied molecular orbital (HOMO) of the HTL
$\mathrm{VBM_H}$	Valence band maximum (VBM) of the HTL
$\mathrm{LUMO_E}$	LUMO of the ETL
$\mathrm{HOMO_E}$	HOMO of the ETL
$\mathrm{CBM_E}$	CBM of the ETL
$\mathrm{VBM_E}$	VBM of the ETL
$\mathrm{LUMO_{dA}}$	LUMO of the donor of the active layer
$\mathrm{HOMO_{dA}}$	HOMO of the donor of the active layer
$\mathrm{LUMO_{aA}}$	LUMO of the acceptor of the active layer
$\mathrm{HOMO_{aA}}$	HOMO of the acceptor of the active layer
E_g	Effective band gap
E_Fa	Fermi level of the anode
E_Fc	Fermi level of the cathode
E_FH	Fermi level of the HTL
E_FE	Fermi level of the ETL
L_A	Thickness of the active layer
L_H	Thickness of the HTL
L_E	Thickness of the ETL
q	Elementary charge
J_nA	Electron current density in the active layer
J_pA	Hole current density in the active layer
G_n	Electron generation rate per unit volume
G_p	Hole generation rate per unit volume
R_n	Net nongeminate recombination rate per unit volume for electrons
R_p	Net nongeminate recombination rate per unit volume for holes
n_A	Free electron concentration in the active layer
p_A	Free hole concentration in the active layer
t	Time
μ_nA	Electron mobility in the active layer
μ_pA	Hole mobility in the active layer
F_A	Electric field in the active layer
D_nA	Electron diffusion coefficient in the active layer
D_pA	Hole diffusion coefficient in the active layer
k_B	Boltzmann constant
T	Absolute temperature
R_b	Net bimolecular recombination rate per unit volume
R_trap	Net trap-assisted recombination rate per unit volume
R_A	Net Auger recombination rate per unit volume
P_d	Charge-transfer (CT) state dissociation probability
G_CT	CT state photogeneration rate per unit volume
k_d	CT state dissociation rate coefficient
k_f	CT state decay rate coefficient
$\mu_\mathrm{nA,act}$	Actual electron mobility in the active layer
$\mu_\mathrm{pA,act}$	Actual hole mobility in the active layer
λ	Donor–acceptor morphology parameter
a	Electron–hole separation of the CT state
$\Delta\psi$	Potential difference
ψ	Electric potential

Table 1 (continued)

Symbol	Description
V_{bi}	Built-in voltage
F_H	Electric field in the HTL
F_E	Electric field in the ETL
V_a	Applied voltage
N_{caA}	Effective density of states (DoS) in the conduction band of the acceptor of the active layer
N_{vdA}	Effective DoS in the valence band of the donor of the active layer
J_{nH}	Electron current density in the HTL
J_{pH}	Hole current density in the HTL
μ_{nH}	Electron mobility in the HTL
μ_{pH}	Hole mobility in the HTL
n_H	Free electron concentration in the HTL
p_H	Free hole concentration in the HTL
D_{nH}	Electron diffusion coefficient in the HTL
D_{pH}	Hole diffusion coefficient in the HTL
N_{cH}	Effective DoS in the conduction band of the HTL
E_{nqF}	Quasi-Fermi level for electrons
N_{vH}	Effective DoS in the valence band of the HTL
E_{pqF}	Quasi-Fermi level for holes
J_{nE}	Electron current density in the ETL
J_{pE}	Hole current density in the ETL
μ_{nE}	Electron mobility in the ETL
μ_{pE}	Hole mobility in the ETL
n_E	Free electron concentration in the ETL
p_E	Free hole concentration in the ETL
D_{nE}	Electron diffusion coefficient in the ETL
D_{pE}	Hole diffusion coefficient in the ETL
N_{cE}	Effective DoS in the conduction band of the ETL
N_{vE}	Effective DoS in the valence band of the ETL
$n_{A,max}$	Maximum electron concentration in the active layer
$p_{A,max}$	Maximum hole concentration in the active layer
$n_{A,net}$	Net electron concentration in the active layer
$p_{A,net}$	Net hole concentration in the active layer
J	Total current density
γ	Bimolecular recombination reduction coefficient
k_L	Langevin recombination coefficient
ϵ_A	Effective permittivity of the active layer
n_0	The solution to $\partial J_{nA}/\partial x = 0$
p_0	The solution to $\partial J_{pA}/\partial x = 0$
n_{int}	Intrinsic carrier concentration
v_{th}	Electron thermal velocity
σ_n	Electron capture cross section
σ_p	Hole capture cross section
N_{trap}	Trap density
E_{trap}	Trap energy level
k_{A1} and k_{A2}	Auger recombination coefficients

levels should be as well-aligned as possible, otherwise the electric field inside the device, and hence the current output and the PCE would not be maximized.

Inside the active layer, the electron and the hole continuity equations at steady state are given by [8, 11]

$$\frac{1}{q}\frac{\partial J_{\mathrm{nA}}}{\partial x} + G_{\mathrm{n}} - R_{\mathrm{n}} = \frac{\partial n_{\mathrm{A}}}{\partial t} = 0 \tag{1}$$

$$-\frac{1}{q}\frac{\partial J_{\mathrm{pA}}}{\partial x} + G_{\mathrm{p}} - R_{\mathrm{p}} = \frac{\partial p_{\mathrm{A}}}{\partial t} = 0 \tag{2}$$

where q is the elementary charge, J_{nA} (J_{pA}) is the electron (hole) current density in the active layer, G_{n} (G_{p}) is the free electron (hole) generation rate per unit volume in the active layer, R_{n} (R_{p}) is the net nongeminate recombination rate per unit volume for electrons (holes) in the active layer, and n_{A} (p_{A}) is the free electron (hole) concentration in the active layer. We assume the carrier photogeneration (carrier generation due to light absorption) only occurs in the active layer, and hence the subscript A (used to denote processes or properties associated with the active layer) is not needed for G_{n} and G_{p} since G_{n} and G_{p} are exclusive for the active layer. Furthermore, we apply the result from Ref. [12] which states that the net carrier recombination rate inside a semiconducting layer is zero if the carrier photogeneration inside the layer is zero. This statement means that only the net nongeminate recombination rate inside the active layer is not zero, whereas the net nongeminate recombination rates inside the HTL and ETL are zero (because there are no carrier photogenerations inside the HTL and ETL), and hence the subscript A is also dropped for R_{n} and R_{p} since R_{n} and R_{p} are exclusive for the active layer.

J_{nA} and J_{pA}, which contain the drift and the diffusion components, are given by [8, 11]

$$J_{\mathrm{nA}} = q\mu_{\mathrm{nA}}F_{\mathrm{A}}n_{\mathrm{A}} + qD_{\mathrm{nA}}\frac{\partial n_{\mathrm{A}}}{\partial x} \tag{3}$$

$$J_{\mathrm{pA}} = q\mu_{\mathrm{pA}}F_{\mathrm{A}}p_{\mathrm{A}} - qD_{\mathrm{pA}}\frac{\partial p_{\mathrm{A}}}{\partial x} \tag{4}$$

where μ_{nA} (μ_{pA}) is the electron (hole) mobility inside the active layer, F_{A} is the electric field inside the active layer, and D_{nA} (D_{pA}) is the electron (hole) diffusion coefficient inside the active layer. D_{nA} and D_{pA} are given by

$$D_{\mathrm{nA}} = \frac{\mu_{\mathrm{nA}}k_{\mathrm{B}}T}{q} \tag{5}$$

$$D_{\mathrm{pA}} = \frac{\mu_{\mathrm{pA}}k_{\mathrm{B}}T}{q} \tag{6}$$

where k_{B} is the Boltzmann constant and T is the absolute temperature.

R_{n} and R_{p} are given by [8, 12]

$$R_{\mathrm{n}} = R_{\mathrm{p}} = R_{\mathrm{b}} + R_{\mathrm{trap}} + R_{\mathrm{A}} \tag{7}$$

where R_{b} is the net bimolecular recombination rate per unit volume, R_{trap} is the net trap-assisted recombination rate per unit volume, and R_{A} is the net Auger recombination rate per unit volume.

Free carriers are produced from the dissociation of CT states, and hence G_{n} and G_{p} are given by [8, 12]

$$G_{\mathrm{n}} = G_{\mathrm{p}} = P_{\mathrm{d}}\left(G_{\mathrm{CT}} + R_{\mathrm{b}}\right) \tag{8}$$

where P_{d} is the CT state dissociation probability, and G_{CT} is the CT state photogeneration rate per unit volume. Note that $\mathrm{R_b}$ reproduces CT states as explained earlier in this section. It is also worth noting that if there is no carrier photogeneration in the active layer, then $R_{\mathrm{b}} = 0$ according to Ref. [12] [this result is explained earlier after Eqs. (1) and (2)]. Furthermore, due to the bulk heterojunction structure of the active layer, the photogenerated excitons can be assumed to immediately reach the donor–acceptor interface and immediately produce CT states. Therefore, it is reasonable to assume that the G_{CT} profile has the same shape as the light absorption profile [8].

The CT state dissociation probability P_{d} is defined as [8, 11, 13]

$$P_{\mathrm{d}} = \frac{k_{\mathrm{d}}}{k_{\mathrm{d}} + k_{\mathrm{f}}} \tag{9}$$

where k_{d} is the CT state dissociation rate coefficient, and k_{f} is the CT state decay rate coefficient. As in our previous J-V model [8], we use k_{d} as described by Ref. [14], which is an improved version of the Onsager-Braun model [13], where parameters such as the actual electron mobility in the active layer $\mu_{\mathrm{nA,act}}$, the actual hole mobility in the active layer $\mu_{\mathrm{pA,act}}$, the donor–acceptor morphology parameter λ, and the electron–hole separation of the CT state a, are required.

It is worth mentioning that the carrier mobilities, temperatures, and electric fields inside the active layer, HTL, and ETL are taken to be uniform (i.e., independent of the position x) in this paper. This is done to allow us to derive analytical expressions for the boundary conditions and to allow us to use the combined analytical and regression method as proposed in Ref. [8].

2.2 Electric fields in the device

In this section, we formulate the approximate electric fields in the active layer, HTL, and ETL for various device settings. As is often the case for OSCs, the active layer is made of undoped or intrinsic organic semiconductors. The HTL and ETL can be made of semiconductors that basically contain no mobile carriers (primarily undoped organic semiconductors [15]) or semiconductors that contain mobile carriers (e.g., metal oxides). As mentioned earlier, we need to approximate the electric fields to be uniform in order to derive analytical expressions for the

boundary conditions and obtain the intended J-V model. To approximate the electric fields, we use the fact that the average electric field across any layer of interest is equal to $-\Delta\psi / L$ where $\Delta\psi$ is the difference in the electric potential ψ across the layer and L is the thickness of the layer [11, 16].

2.2.1 Device with the HTL and ETL made of semiconductors without mobile carriers

When a semiconductor that contains no mobile carriers (usually undoped organic semiconductor) makes contact with a material that contains mobile carriers (e.g., a metal), exchanges of free of carriers generally do not occur (and thus no depletion region exists) at the contact between the two materials even if the Fermi levels of the two materials are different. Hence, a semiconductor without mobile carriers can be treated like an insulator (instead of a semiconductor) when it makes contact with another material (whether the material contains mobile carriers or not). This fact leads to the well-known metal–insulator-metal model used for describing the basic OSC structure which consists of an organic active layer sandwiched between two electrodes [17].

For the device with the HTL and ETL made of semiconductors without mobile carriers, the device can therefore be viewed as a metal (anode)-insulator (HTL)-insulator (organic active layer)-insulator (ETL)-metal (cathode) structure, where the positions of the interfaces are as shown in Fig. 1. There are no depletion regions at all interfaces including at the anode-HTL (metal–insulator) and ETL-cathode (insulator–metal) interfaces. To formulate the electric fields, we can view the HTL, active layer, and ETL as a single insulator sandwiched by the anode and cathode. The built-in voltage V_{bi} across any specific layer is given by the potential difference $\Delta\psi$ across the layer without applied bias. Hence, V_{bi} across the HTL, active layer, and ETL is given by (refer Fig. 1)

$$V_{\mathrm{bi}} = \psi|_{x=L_{\mathrm{A}}+L_{\mathrm{E}}} - \psi|_{x=-L_{\mathrm{H}}} = \frac{E_{\mathrm{Fc}} - E_{\mathrm{Fa}}}{q} \tag{10}$$

By considering the effect of the applied voltage V_{a}, the potential difference $\Delta\psi$ across the HTL, active layer, and ETL is now given by $V_{\mathrm{bi}} - V_{\mathrm{a}}$ (positive V_{a} means forward bias, which opposes V_{bi}, while negative V_{a} means reverse bias). Since we view the HTL, active layer, and ETL as a single insulator layer, we can assume that F_{H}, F_{A}, and F_{E} to be the same and are given by the average electric field across that single layer, where F_{H}, F_{A}, and F_{E} are the electric fields inside the HTL, active layer, and ETL, respectively. Therefore, F_{H}, F_{A}, and F_{E} can be approximated to be given by

$$F_{\mathrm{H}} = F_{\mathrm{A}} = F_{\mathrm{E}} = \frac{V_{\mathrm{a}} - V_{\mathrm{bi}}}{L_{\mathrm{H}} + L_{\mathrm{A}} + L_{\mathrm{E}}} \tag{11}$$

where V_{bi} is given by Eq. (10).

2.2.2 Device with the HTL made of a semiconductor without mobile carriers and no ETL

For the device in this case, the anode-HTL, HTL-active layer, and active layer-cathode interfaces are located at $x = -L_{\mathrm{H}}$, $x = 0$, and $x = L_{\mathrm{A}}$, respectively (refer Fig. 1). As explained in Sect. 2.2.1, the device in this case can be viewed as a metal (anode)-insulator (HTL)-insulator (organic active layer)-metal (cathode) structure. There are no depletion regions at all interfaces. To formulate F_{H} and F_{A}, we can view the HTL and active layer as a single insulator sandwiched by the anode and cathode. The built-in voltage across the HTL and active layer is given by

$$V_{\mathrm{bi}} = \psi|_{x=L_{\mathrm{A}}} - \psi|_{x=-L_{\mathrm{H}}} = \frac{E_{\mathrm{Fc}} - E_{\mathrm{Fa}}}{q} \tag{12}$$

Considering the effect of V_{a}, the potential difference $\Delta\psi$ across the HTL and active layer is given by $V_{\mathrm{bi}} - V_{\mathrm{a}}$. Since we view the HTL and the active layer as a single insulator layer, we can assume that F_{H} and F_{A} to be the same and are given by the average electric field across that single layer, which can be approximated to be given by

$$F_{\mathrm{H}} = F_{\mathrm{A}} = \frac{V_{\mathrm{a}} - V_{\mathrm{bi}}}{L_{\mathrm{H}} + L_{\mathrm{A}}} \tag{13}$$

where V_{bi} is given by Eq. (12).

2.2.3 Device with the ETL made of a semiconductor without mobile carriers and no HTL

For the device in this case, the anode-active layer, active layer-ETL, and ETL-cathode interfaces are located at $x = 0$, $x = L_{\mathrm{A}}$ and $x = L_{\mathrm{A}} + L_{\mathrm{E}}$, respectively (refer Fig. 1). As explained in Sect. 2.2.1, the device in this case can be viewed as a metal (anode)-insulator (organic active layer)-insulator (ETL)-metal (cathode) structure, where there are no depletion regions at all of those interfaces. To formulate F_{A} and F_{E}, we can view the active layer and ETL as a single insulator sandwiched by the anode and cathode. The built-in voltage across the active layer and ETL is given by

$$V_{\mathrm{bi}} = \psi|_{x=L_{\mathrm{A}}+L_{\mathrm{E}}} - \psi|_{x=0} = \frac{E_{\mathrm{Fc}} - E_{\mathrm{Fa}}}{q} \tag{14}$$

Considering the effect of V_{a}, the potential difference $\Delta\psi$ across the active layer and ETL is given by $V_{\mathrm{bi}} - V_{\mathrm{a}}$. Since we view the active layer and ETL as a single layer, we can assume that F_{A} and F_{E} to be the same and are given by the average electric field across that single layer, which can be approximated to be given by

$$F_A = F_E = \frac{V_a - V_{bi}}{L_A + L_E} \tag{15}$$

where V_{bi} is given by Eq. (14).

2.2.4 Device with the HTL and ETL made of semiconductors with mobile carriers

As explained in Sect. 2.2.1, the device in this case can be viewed as a metal (anode)-semiconductor (HTL)-insulator (organic active layer)-semiconductor (ETL)-metal (cathode) structure, where the positions of the interfaces are as shown in Fig. 1. Obviously, there are no depletion regions at the HTL-active layer (semiconductor-insulator) and active layer-ETL (insulator-semiconductor) interfaces. However, at the anode-HTL (ETL-cathode) interface, a mismatch between E_{Fa} (E_{FE}) and E_{FH} (E_{Fc}) leads to a depletion region. If $E_{Fa} > E_{FH}$ ($E_{FE} > E_{Fc}$), a hole (an electron) Schottky barrier forms at the anode-HTL (ETL-cathode) interface which can disrupt the working operation by disrupting the collection of free holes (electrons) by the anode (cathode). Therefore, it is essential to ensure that any mismatch between E_{Fa} (E_{FE}) and E_{FH} (E_{Fc}) does not disrupt the device operation.

A CTL must be a semiconductor (in other words, a material with a band gap) in order to perform the role of blocking the unwanted carrier type. Therefore, to ensure that the use of the HTL (ETL) serves its purposes well, i.e., to efficiently transport free holes (electrons) and block free electrons (holes) and excitons, we only consider the case where the HTL (ETL) is a strong p-type (n-type) semiconductor if the HTL (ETL) is made of a semiconductor with mobile carriers. This is because a strong p-type (n-type) semiconductor to a certain extent can be treated similar to a metal [18], which means that the depletion layer in a strong p-type (n-type) semiconductor can often be neglected [18] and this can ensure that any mismatch between E_{Fa} (E_{FE}) and E_{FH} (E_{Fc}) does not disrupt the device operation. Of course, technically a very thin depletion layer still appears at the anode-HTL (ETL-cathode) interface if the HTL (ETL) is a strong p-type (n-type) semiconductor and if there is a mismatch between E_{Fa} (E_{Fc}) and E_{FH} (E_{FE}). However, even if a hole (an electron) Schottky barrier exists due to the energy level mismatch, the very thin depletion layer still allows free holes (electrons) to tunnel easily from the valence (conduction) band of the HTL (ETL) to the anode (cathode), and this means that the anode (cathode) can still collect free holes (electrons) efficiently. As widely known, metals are usually assumed to be ideal conductors in electrical circuit analysis (which is reasonable due to their very high conductivity), meaning that the potential difference across metals is usually assumed to be zero (in reality, metals are of course not ideal conductors). Therefore, since the HTL (ETL) is a strong p-type (n-type) semiconductor, we assume that the potential difference $\Delta\psi$ across the HTL (ETL) is not influenced by V_a and is always zero, just like how the potential difference across a metal is usually assumed to be. Therefore, for the device in this case, we can approximate that

$$F_H = F_E = 0 \tag{16}$$

For the active layer, the built-in voltage across it (i.e., $\Delta\psi$ across it in the absence of V_a) is given by

$$V_{bi} = \psi|_{x=L_A} - \psi|_{x=0} = \frac{E_{FE} - E_{FH}}{q} \tag{17}$$

Since V_a only affects $\Delta\psi$ across the active layer (because it does not affect $\Delta\psi$ across the HTL and ETL), $\Delta\psi$ across the active layer is therefore given by $V_{bi} - V_a$. Therefore, we can approximate F_A to be

$$F_A = \frac{V_a - V_{bi}}{L_A} \tag{18}$$

where V_{bi} is given by Eq. (17).

2.2.5 Device with the HTL made of a semiconductor with mobile carriers and no ETL

For the device in this case, the anode-HTL, HTL-active layer, and active layer-cathode interfaces are located at $x = -L_H$, $x = 0$, and $x = L_A$, respectively (refer Fig. 1). As explained in Sect. 2.2.1, the device in this case can be viewed as a metal (anode)-semiconductor (HTL)-insulator (organic active layer)-metal (cathode) structure. As explained in Sect. 2.2.4, the HTL is considered to be a strong p-type semiconductor. There are no depletion layers at all interfaces, including at the anode-HTL interface (negligible depletion layer) as explained in Sect. 2.2.4. Using the same argument as in Sect. 2.2.4 above, we can assume that $\Delta\psi$ across the HTL made of a strong p-type semiconductor is not influenced by V_a and is always zero, and hence

$$F_H = 0 \tag{19}$$

The built-in voltage (i.e., $\Delta\psi$ without V_a) across the active layer is given by

$$V_{bi} = \psi|_{x=L_A} - \psi|_{x=0} = \frac{E_{Fc} - E_{FH}}{q} \tag{20}$$

Since V_a only affects $\Delta\psi$ across the active layer for the device in this case, $\Delta\psi$ across the active layer is $V_{bi} - V_a$. Therefore, we can approximate F_A to be given by

$$F_A = \frac{V_a - V_{bi}}{L_A} \tag{21}$$

where V_{bi} is given by Eq. (20).

2.2.6 Device with the ETL made of a semiconductor with mobile carriers and no HTL

For the device in this case, the anode-active layer, active layer-ETL, and ETL-cathode interfaces are located at $x = 0$, $x = L_A$, and $x = L_A + L_E$, respectively (refer Fig. 1). As explained in Sect. 2.2.1, the device in this case can be viewed as a metal (anode)-insulator (organic active layer)-semiconductor (ETL)-metal (cathode) structure. As explained in Sect. 2.2.4, the ETL is considered to be a strong n-type semiconductor. There are no depletion layers at all interfaces, including at the ETL-cathode interface (negligible depletion layer) as explained in Sect. 2.2.4. Using the same argument as in Sect. 2.2.4 above, we can assume that $\Delta\psi$ across the ETL made of a strong n-type semiconductor is not influenced by V_a and is always zero, and hence

$$F_E = 0 \tag{22}$$

The built-in voltage (i.e., $\Delta\psi$ without V_a) across the active layer is given by

$$V_{bi} = \psi|_{x=L_A} - \psi|_{x=0} = \frac{E_{FE} - E_{Fa}}{q} \tag{23}$$

Since V_a only affects $\Delta\psi$ across the active layer for the device in this case, $\Delta\psi$ across the active layer is $V_{bi} - V_a$. Therefore, we can approximate F_A to be given by

$$F_A = \frac{V_a - V_{bi}}{L_A} \tag{24}$$

where V_{bi} is given by Eq. (23).

2.2.7 Device with the HTL made of a semiconductor without mobile carriers and the ETL made of a semiconductor with mobile carriers

As explained in Sect. 2.2.1, the device in this case can be viewed as a metal (anode)-insulator (HTL)-insulator (organic active layer)-semiconductor (ETL)-metal (cathode) structure, where the positions of the interfaces are as shown in Fig. 1. As explained in Sect. 2.2.4, the ETL is considered to be a strong n-type semiconductor. There are no depletion layers at all interfaces, including at the ETL-cathode interface (negligible depletion layer) as explained in Sect. 2.2.4. Using the same argument as in Sect. 2.2.4 above, we can assume that $\Delta\psi$ across the ETL made of a strong n-type semiconductor is not influenced by V_a and is always zero, and hence

$$F_E = 0 \tag{25}$$

To formulate F_H and F_A, we can treat the HTL and active layer as a single insulator. The built-in voltage (i.e., $\Delta\psi$ without V_a) across the HTL and active layer is given by

$$V_{bi} = \psi|_{x=L_A} - \psi|_{x=-L_H} = \frac{E_{FE} - E_{Fa}}{q} \tag{26}$$

Since V_a only affects $\Delta\psi$ across the HTL and active layer for the device in this case, $\Delta\psi$ across the HTL and active layer is $V_{bi} - V_a$. Since we view the HTL and active layer as a single layer, we can assume that F_H and F_A to be the same and are given by the average electric field across that single layer, which can be approximated to be given by

$$F_H = F_A = \frac{V_a - V_{bi}}{L_H + L_A} \tag{27}$$

where V_{bi} is given by Eq. (26).

2.2.8 Device with the HTL made of a semiconductor with mobile carriers and the ETL made of a semiconductor without mobile carriers

As explained in Sect. 2.2.1, the device in this case can be viewed as a metal (anode)-semiconductor (HTL)-insulator (organic active layer)-insulator (ETL)-metal (cathode) structure, where the positions of the interfaces are as shown in Fig. 1. As explained in Sect. 2.2.4, the HTL is considered to be a strong p-type semiconductor. There are no depletion layers at all interfaces, including at the anode-HTL interface (negligible depletion layer) as explained in Sect. 2.2.4. Using the same argument as in Sect. 2.2.4 above, we can assume that $\Delta\psi$ across the HTL made of a strong p-type semiconductor is not influenced by V_a and is always zero, and hence

$$F_H = 0 \tag{28}$$

To formulate F_A and F_E, we can treat the active layer and ETL as a single insulator. The built-in voltage (i.e., $\Delta\psi$ without V_a) across the active layer and ETL is given by

$$V_{bi} = \psi|_{x=L_A+L_E} - \psi|_{x=0} = \frac{E_{Fc} - E_{FH}}{q} \tag{29}$$

Since V_a only affects $\Delta\psi$ across the active layer and ETL for the device in this case, $\Delta\psi$ across the active layer and ETL is $V_{bi} - V_a$. Since we view the active layer and ETL as a single layer, we can assume that F_A and F_E to be the same and are given by the average electric field across that single layer, which can be approximated to be given by

$$F_A = F_E = \frac{V_a - V_{bi}}{L_A + L_E} \tag{30}$$

where V_{bi} is given by Eq. (29).

2.3 Boundary conditions

The aims of this Sect. 2.3 are to derive the boundary conditions at $x = 0$ and $x = L_A$ for Eqs. (1) and (2) for different device settings, where Eqs. (1) and (2) are the continuity equations for the electrons and the holes in the active layer, respectively. In other words, here we aim to derive the boundary conditions that describe n_A and p_A at $x = 0$ and $x = L_A$ for different device settings.

2.3.1 Boundary conditions at $x = 0$ for the device without the HTL

For an OSC without the HTL, $x = 0$ is the position of the anode-active layer contact (refer Fig. 1). At $x = 0$, there is no depletion layer (because it is a metal–insulator contact as explained in Sect. 2.2.1), and both the electron and the hole quasi-Fermi levels must coincide with E_{Fa}. Employing the Boltzmann statistics, the boundary conditions at $x = 0$ are [8, 11]

$$n_A\big|_{x=0} = N_{caA} \exp\left[\frac{-\left(\mathrm{LUMO}_{aA} - E_{Fa}\right)}{k_B T}\right] \tag{31}$$

$$p_A\big|_{x=0} = N_{vdA} \exp\left[\frac{-\left(E_{Fa} - \mathrm{HOMO}_{dA}\right)}{k_B T}\right] \tag{32}$$

where N_{caA} is the effective density of states (DoS) in the conduction band of the acceptor material of the active layer and N_{vdA} is effective DoS in the valence band of the donor material of the active layer.

2.3.2 Boundary conditions at $x = L_A$ for the device without the ETL

For an OSC without the ETL, $x = L_A$ is the position of the active layer-cathode contact (refer Fig. 1). At $x = L_A$, there is no depletion layer (because it is an insulator–metal contact as explained in Sect. 2.2.1), and both the electron and the hole quasi-Fermi levels must coincide with E_{Fc}. Employing the Boltzmann statistics, the boundary conditions at $x = L_A$ are [8, 11]

$$n_A\big|_{x=L_A} = N_{caA} \exp\left[\frac{-\left(\mathrm{LUMO}_{aA} - E_{Fc}\right)}{k_B T}\right] \tag{33}$$

$$p_A\big|_{x=L_A} = N_{vdA} \exp\left[\frac{-\left(E_{Fc} - \mathrm{HOMO}_{dA}\right)}{k_B T}\right] \tag{34}$$

2.3.3 Boundary conditions at $x = 0$ for the device with the HTL made of a semiconductor without mobile carriers

An HTL without mobile carriers is made of an organic semiconductor (usually undoped), and hence, LUMO_H and HOMO_H are used in this Sect. 2.3.3 instead of CBM_H and VBM_H. The anode-HTL and the HTL-active layer interfaces are located at $x = -L_H$ and $x = 0$, respectively (see Fig. 1), and can be treated like metal–insulator and insulator-insulator contacts, respectively (see the explanation in Sect. 2.2.1). The electron current density inside the HTL, denoted by J_{nH}, and the hole current density inside the HTL, denoted by J_{pH}, are given by

$$J_{nH} = q\mu_{nH}F_H n_H + qD_{nH}\frac{\partial n_H}{\partial x} \tag{35}$$

$$J_{pH} = q\mu_{pH}F_H p_H - qD_{pH}\frac{\partial p_H}{\partial x} \tag{36}$$

where n_H (p_H) is the free electron (hole) concentration inside the HTL, μ_{nH} (μ_{pH}) is the electron (hole) mobility inside the HTL, F_H is the electric field inside the HTL, and D_{nH} (D_{pH}) is the electron (hole) diffusion coefficient inside the HTL.

The continuity equation for electrons in the HTL has a similar form to Eq. (1). As mentioned in Sect. 2.1, we assume that the carrier mobilities, temperatures, and electric fields (and hence the diffusion coefficients too) inside all layers to be uniform, and we also assume that the carrier photogeneration rate and the net nongeminate recombination rate in the HTL to be zero. Therefore, the continuity equation for electrons in the HTL at steady state is

$$\frac{1}{q}\frac{\partial J_{nH}}{\partial x} = D_{nH}\frac{\partial^2 n_H}{\partial x^2} + \mu_{nH}F_H\frac{\partial n_H}{\partial x} = 0 \tag{37}$$

The general solution to Eq. (37) is

$$n_H = A_1 \exp\left(\frac{-\mu_{nH}F_H x}{D_{nH}}\right) + A_2 \tag{38}$$

where A_1 and A_2 are constants that can be obtained by applying the boundary conditions, one at $x = -L_H$ and the other at $x = 0$. At $x = -L_H$, the electron quasi-Fermi level must coincide with E_{Fa}, and thus by using the Boltzmann statistics, the boundary condition for Eq. (37) at $x = -L_H$ is

$$n_H\big|_{x=-L_H} = N_{cH} \exp\left[\frac{-\left(\mathrm{LUMO}_H - E_{Fa}\right)}{k_B T}\right] \tag{39}$$

where N_{cH} is the effective DoS in the conduction band of the HTL. At $x = 0$, the electron concentration in the HTL is

$$n_{\mathrm{H}}\big|_{x=0} = N_{\mathrm{cH}} \exp\left[\frac{-\left(\mathrm{LUMO_H} - E_{\mathrm{nqF}}\big|_{x=0}\right)}{k_{\mathrm{B}}T}\right] \tag{40}$$

where E_{nqF} is the electron quasi-Fermi level. Since E_{nqF} must be continuous within the device, $E_{\mathrm{nqF}}\big|_{x=0}$ in the HTL must be the same as $E_{\mathrm{nqF}}\big|_{x=0}$ in the active layer. Therefore, at $x = 0$, the electron concentration in the active layer is

$$n_{\mathrm{A}}\big|_{x=0} = N_{\mathrm{caA}} \exp\left[\frac{-\left(\mathrm{LUMO_{aA}} - E_{\mathrm{nqF}}\big|_{x=0}\right)}{k_{\mathrm{B}}T}\right] \tag{41}$$

Combining Eqs. (40) and (41), we get another boundary condition for Eq. (37), which is at $x = 0$, and is given by

$$n_{\mathrm{H}}\big|_{x=0} = \alpha_1 \, n_{\mathrm{A}}\big|_{x=0} \tag{42}$$

where

$$\alpha_1 = \frac{N_{\mathrm{cH}}}{N_{\mathrm{caA}}} \exp\left(\frac{\mathrm{LUMO_{aA}} - \mathrm{LUMO_H}}{k_{\mathrm{B}}T}\right) \tag{43}$$

Applying the two boundary conditions [i.e., Eqs. (39) and (42)] to the solution of Eq. (37) [i.e., Eq. (38)], we get

$$A_1 = \frac{n_{\mathrm{H}}\big|_{x=-L_{\mathrm{H}}} - n_{\mathrm{H}}\big|_{x=0}}{\beta_1} \tag{44}$$

$$A_2 = \frac{n_{\mathrm{H}}\big|_{x=0} \exp\left(\frac{\mu_{\mathrm{nH}} F_{\mathrm{H}} L_{\mathrm{H}}}{D_{\mathrm{nH}}}\right) - n_{\mathrm{H}}\big|_{x=-L_{\mathrm{H}}}}{\beta_1} \tag{45}$$

with

$$\beta_1 = \exp\left(\frac{\mu_{\mathrm{nH}} F_{\mathrm{H}} L_{\mathrm{H}}}{D_{\mathrm{nH}}}\right) - 1 \tag{46}$$

where $n_{\mathrm{H}}\big|_{x=-L_{\mathrm{H}}}$ and $n_{\mathrm{H}}\big|_{x=0}$ are given by Eqs. (39) and (42), respectively.

Furthermore, the electron current continuity at $x = 0$ means that $J_{\mathrm{nH}}\big|_{x=0} = J_{\mathrm{nA}}\big|_{x=0}$ where J_{nH} and J_{nA} are given by Eqs. (35) and (3), respectively. Applying the electron current continuity at $x = 0$ interface, we have

$$\mu_{\mathrm{nH}} F_{\mathrm{H}} \, n_{\mathrm{H}}\big|_{x=0} + D_{\mathrm{nH}} \left.\frac{\partial n_{\mathrm{H}}}{\partial x}\right|_{x=0} = \mu_{\mathrm{nA}} F_{\mathrm{A}} \, n_{\mathrm{A}}\big|_{x=0} + D_{\mathrm{nA}} \left.\frac{\partial n_{\mathrm{A}}}{\partial x}\right|_{x=0} \tag{47}$$

We can replace $\left(\partial n_{\mathrm{H}} / \partial x\right)\big|_{x=0}$ and $n_{\mathrm{H}}\big|_{x=0}$ in Eq. (47) with the derivative of Eq. (38) at $x = 0$ and Eq. (42), respectively, to obtain the boundary condition at $x = 0$ for Eq. (1), which is given by

$$\left[\mu_{\mathrm{nH}} F_{\mathrm{H}} \alpha_1 \exp\left(\frac{\mu_{\mathrm{nH}} F_{\mathrm{H}} L_{\mathrm{H}}}{D_{\mathrm{nH}}}\right) - \mu_{\mathrm{nA}} F_{\mathrm{A}} \beta_1\right] n_{\mathrm{A}}\big|_{x=0} - \beta_1 D_{\mathrm{nA}} \left.\frac{\partial n_{\mathrm{A}}}{\partial x}\right|_{x=0} = \mu_{\mathrm{nH}} F_{\mathrm{H}} \, n_{\mathrm{H}}\big|_{x=-L_{\mathrm{H}}} \tag{48}$$

where $n_{\mathrm{H}}\big|_{x=-L_{\mathrm{H}}}$ is given by Eq. (39).

To obtain the boundary condition at $x = 0$ for Eq. (2), we start with the continuity equation for free holes in the HTL at steady state [which has a similar form to Eq. (2), but with zero carrier photogeneration rate and zero net nongeminate recombination rate as explained in Sect. 2.1, which is

$$-\frac{1}{q}\frac{\partial J_{\mathrm{pH}}}{\partial x} = D_{\mathrm{pH}} \frac{\partial^2 p_{\mathrm{H}}}{\partial x^2} - \mu_{\mathrm{pH}} F_{\mathrm{H}} \frac{\partial p_{\mathrm{H}}}{\partial x} = 0 \tag{49}$$

The general solution to Eq. (49) is

$$p_{\mathrm{H}} = A_3 \exp\left(\frac{\mu_{\mathrm{pH}} F_{\mathrm{H}} x}{D_{\mathrm{pH}}}\right) + A_4 \tag{50}$$

where A_3 and A_4 are constants that can be obtained by applying the boundary conditions, one at $x = -L_{\mathrm{H}}$ and another at $x = 0$. At $x = -L_{\mathrm{H}}$, the hole quasi-Fermi level must coincide with E_{Fa}, and thus by using the Boltzmann statistics, the boundary condition for Eq. (49) at $x = -L_{\mathrm{H}}$ is

$$p_{\mathrm{H}}\big|_{x=-L_{\mathrm{H}}} = N_{\mathrm{vH}} \exp\left[\frac{-\left(E_{\mathrm{Fa}} - \mathrm{HOMO_H}\right)}{k_{\mathrm{B}}T}\right] \tag{51}$$

where N_{vH} is the effective DoS in the valence band of the HTL. At $x = 0$, the hole concentration in the HTL is

$$p_{\mathrm{H}}\big|_{x=0} = N_{\mathrm{vH}} \exp\left[\frac{-\left(E_{\mathrm{pqF}}\big|_{x=0} - \mathrm{HOMO_H}\right)}{k_{\mathrm{B}}T}\right] \tag{52}$$

where E_{pqF} is the hole quasi-Fermi level. Since E_{pqF} must be continuous within the device, $E_{\mathrm{pqF}}\big|_{x=0}$ in the HTL must be the same as $E_{\mathrm{pqF}}\big|_{x=0}$ in the active layer. Therefore, at $x = 0$, the hole concentration in the active layer is

$$p_{\mathrm{A}}\big|_{x=0} = N_{\mathrm{vdA}} \exp\left[\frac{-\left(E_{\mathrm{pqF}}\big|_{x=0} - \mathrm{HOMO_{dA}}\right)}{k_{\mathrm{B}}T}\right] \tag{53}$$

Combining Eqs. (52) and (53), we get another boundary condition for Eq. (49), which is at $x = 0$, and is given by

$$p_{\mathrm{H}}\big|_{x=0} = \alpha_2 \, p_{\mathrm{A}}\big|_{x=0} \tag{54}$$

where

$$\alpha_2 = \frac{N_{vH}}{N_{vdA}} \exp\left(\frac{\mathrm{HOMO_H} - \mathrm{HOMO_{dA}}}{k_B T}\right) \tag{55}$$

Applying the two boundary conditions [i.e., Eqs. (51) and (54)] to the solution of Eq. (49) [i.e., Eq. (50)], we get

$$A_3 = \frac{p_H|_{x=-L_H} - p_H|_{x=0}}{\beta_2} \tag{56}$$

$$A_4 = \frac{p_H|_{x=0} \exp\left(\frac{-\mu_{pH} F_H L_H}{D_{pH}}\right) - p_H|_{x=-L_H}}{\beta_2} \tag{57}$$

with

$$\beta_2 = \exp\left(\frac{-\mu_{pH} F_H L_H}{D_{pH}}\right) - 1 \tag{58}$$

where $p_H|_{x=-L_H}$ and $p_H|_{x=0}$ are given by Eqs. (51) and (54), respectively.

Furthermore, the hole current continuity at $x = 0$ means that $J_{pH}\big|_{x=0} = J_{pA}\big|_{x=0}$ where J_{pH} and J_{pA} are given by Eqs. (36) and (4), respectively. Applying the hole current continuity at $x = 0$ interface, we have

$$\mu_{pH} F_H p_H|_{x=0} - D_{pH} \frac{\partial p_H}{\partial x}\bigg|_{x=0} = \mu_{pA} F_A p_A|_{x=0} - D_{pA} \frac{\partial p_A}{\partial x}\bigg|_{x=0} \tag{59}$$

We can replace $\left(\partial p_H / \partial x\right)\big|_{x=0}$ and $p_H|_{x=0}$ in Eq. (59) with the derivative of Eq. (50) at $x = 0$ and Eq. (54), respectively, to obtain the boundary condition at $x = 0$ for Eq. (2), which is given by

$$\left[\mu_{pH} F_H \alpha_2 \exp\left(\frac{-\mu_{pH} F_H L_H}{D_{pH}}\right) - \mu_{pA} F_A \beta_2\right] p_A|_{x=0} + \beta_2 D_{pA} \frac{\partial p_A}{\partial x}\bigg|_{x=0} = \mu_{pH} F_H p_H|_{x=-L_H} \tag{60}$$

where $p_H|_{x=-L_H}$ is given by Eq. (51).

It is worth noting that F_H and F_A can be zero at a certain V_a (note that $F_H = F_A$ for the device in this case as explained in Sect. 2.2.1 or Sect. 2.2.2 for example). When F_H and F_A are zero, $\beta_1 = 0$ [see Eq. (46)] and thus A_1 and A_2 are undefined (the same happens with A_3 and A_4 because $\beta_2 = 0$ too). Nevertheless, when F_H and F_A are zero, Eqs. (48) and (60) can still be used for the device in this case, but by using values for F_H and F_A that are very close to zero, not exactly zero. Alternatively (and more accurately), when F_H and F_A are zero, the boundary conditions at $x = 0$ for Eqs. (1) and (2) for the device in this case are the same as the boundary conditions at $x = 0$ for Eqs. (1) and (2) for the device described in Sect. 2.3.5 (by applying $F_A = 0$ to the boundary conditions obtained in Sect. 2.3.5).

2.3.4 Boundary conditions at $x = L_A$ for the device with the ETL made of a semiconductor without mobile carriers

An ETL without mobile carriers is made of an organic semiconductor (usually undoped), and hence $\mathrm{LUMO_E}$ and $\mathrm{HOMO_E}$ are used here instead of $\mathrm{CBM_E}$ and $\mathrm{VBM_E}$. The active layer-ETL and the ETL-cathode interfaces are located at $x = L_A$ and $x = L_A + L_E$, respectively (see Fig. 1), and can be treated like insulator-insulator and insulator–metal contacts, respectively (see the explanation in Sect. 2.2.1). The electron current density inside the ETL, denoted by J_{nE}, and the hole current density inside the ETL, denoted by J_{pE}, are given by

$$J_{nE} = q\mu_{nE} F_E n_E + q D_{nE} \frac{\partial n_E}{\partial x} \tag{61}$$

$$J_{pE} = q\mu_{pE} F_E p_E - q D_{pE} \frac{\partial p_E}{\partial x} \tag{62}$$

where n_E (p_E) is the free electron (hole) concentration inside the ETL, μ_{nE} (μ_{pE}) is the electron (hole) mobility inside the ETL, F_E is the electric field inside the ETL, and D_{nE} (D_{pE}) is the electron (hole) diffusion coefficient inside the ETL.

The continuity equation for electrons in the ETL has a similar form to Eq. (1). As mentioned in Sect. 2.1, we assume that the carrier mobilities, temperatures, and electric fields (and hence the diffusion coefficients too) inside all layers to be uniform, and we also assume that the carrier photogeneration rate and the net nongeminate recombination rate in the ETL to be zero. Therefore, the continuity equation for electrons in the ETL at steady state is

$$\frac{1}{q}\frac{\partial J_{nE}}{\partial x} = D_{nE}\frac{\partial^2 n_E}{\partial x^2} + \mu_{nE} F_E \frac{\partial n_E}{\partial x} = 0 \tag{63}$$

The general solution to Eq. (63) is

$$n_E = A_5 \exp\left(\frac{-\mu_{nE} F_E x}{D_{nE}}\right) + A_6 \tag{64}$$

where A_5 and A_6 are constants that can be obtained by applying the boundary conditions, one at $x = L_A + L_E$ and another at $x = L_A$. At $x = L_A + L_E$, the electron quasi-Fermi level must coincide with E_{Fc}, and thus by using the Boltzmann statistics, the boundary condition for Eq. (63) at $x = L_A + L_E$ is

$$n_{\mathrm{E}}\big|_{x=L_{\mathrm{A}}+L_{\mathrm{E}}} = N_{\mathrm{cE}} \exp\left[\frac{-\left(\mathrm{LUMO_E} - E_{\mathrm{Fc}}\right)}{k_{\mathrm{B}}T}\right] \tag{65}$$

where N_{cE} is the effective DoS in the conduction band of the ETL. There must be a continuity in the electron quasi-Fermi level inside the device including at $x = L_{\mathrm{A}}$, and by using a similar approach as in Sect. 2.3.3 [refer Eqs. (40) and (41)], it can be shown that the boundary condition for Eq. (63) at $x = L_{\mathrm{A}}$ is

$$n_{\mathrm{E}}\big|_{x=L_{\mathrm{A}}} = \alpha_3\, n_{\mathrm{A}}\big|_{x=L_{\mathrm{A}}} \tag{66}$$

where

$$\alpha_3 = \frac{N_{\mathrm{cE}}}{N_{\mathrm{caA}}} \exp\left(\frac{\mathrm{LUMO_{aA}} - \mathrm{LUMO_E}}{k_{\mathrm{B}}T}\right) \tag{67}$$

Applying the two boundary conditions [i.e., Eqs. (65) and (66)] to the solution of Eq. (63) [i.e., Eq. (64)], we get

$$A_5 = \frac{n_{\mathrm{E}}\big|_{x=L_{\mathrm{A}}+L_{\mathrm{E}}} - n_{\mathrm{E}}\big|_{x=L_{\mathrm{A}}}}{\beta_3} \tag{68}$$

$$A_6 = \frac{n_{\mathrm{E}}\big|_{x=L_{\mathrm{A}}} \exp\left[\frac{-\mu_{\mathrm{nE}}F_{\mathrm{E}}\left(L_{\mathrm{A}}+L_{\mathrm{E}}\right)}{D_{\mathrm{nE}}}\right] - n_{\mathrm{E}}\big|_{x=L_{\mathrm{A}}+L_{\mathrm{E}}} \exp\left(\frac{-\mu_{\mathrm{nE}}F_{\mathrm{E}}L_{\mathrm{A}}}{D_{\mathrm{nE}}}\right)}{\beta_3} \tag{69}$$

with

$$\beta_3 = \exp\left[\frac{-\mu_{\mathrm{nE}}F_{\mathrm{E}}\left(L_{\mathrm{A}}+L_{\mathrm{E}}\right)}{D_{\mathrm{nE}}}\right] - \exp\left(\frac{-\mu_{\mathrm{nE}}F_{\mathrm{E}}L_{\mathrm{A}}}{D_{\mathrm{nE}}}\right) \tag{70}$$

where $n_{\mathrm{E}}\big|_{x=L_{\mathrm{A}}+L_{\mathrm{E}}}$ and $n_{\mathrm{E}}\big|_{x=L_{\mathrm{A}}}$ are given by Eqs. (65) and (66), respectively.

The electron current continuity at $x = L_{\mathrm{A}}$ means that $J_{\mathrm{nE}}\big|_{x=L_{\mathrm{A}}} = J_{\mathrm{nA}}\big|_{x=L_{\mathrm{A}}}$ where J_{nE} and J_{nA} are given by Eqs. (61) and (3), respectively. Applying the electron current continuity at $x = L_{\mathrm{A}}$ interface, we have

$$\mu_{\mathrm{nE}}F_{\mathrm{E}}\, n_{\mathrm{E}}\big|_{x=L_{\mathrm{A}}} + D_{\mathrm{nE}}\left.\frac{\partial n_{\mathrm{E}}}{\partial x}\right|_{x=L_{\mathrm{A}}} = \mu_{\mathrm{nA}}F_{\mathrm{A}}\, n_{\mathrm{A}}\big|_{x=L_{\mathrm{A}}} + D_{\mathrm{nA}}\left.\frac{\partial n_{\mathrm{A}}}{\partial x}\right|_{x=L_{\mathrm{A}}} \tag{71}$$

We can replace $\left(\partial n_{\mathrm{E}}/\partial x\right)\big|_{x=L_{\mathrm{A}}}$ and $n_{\mathrm{E}}\big|_{x=L_{\mathrm{A}}}$ in Eq. (71) with the derivative of Eq. (64) at $x = L_{\mathrm{A}}$ and Eq. (66), respectively, to obtain the boundary condition at $x = L_{\mathrm{A}}$ for Eq. (1), which is given by

$$\left(\mu_{\mathrm{nE}}F_{\mathrm{E}}\alpha_3 \exp\left[\frac{-\mu_{\mathrm{nE}}F_{\mathrm{E}}\left(L_{\mathrm{A}}+L_{\mathrm{E}}\right)}{D_{\mathrm{nE}}}\right] - \mu_{\mathrm{nA}}F_{\mathrm{A}}\beta_3\right) n_{\mathrm{A}}\big|_{x=L_{\mathrm{A}}} - \beta_3 D_{\mathrm{nA}}\left.\frac{\partial n_{\mathrm{A}}}{\partial x}\right|_{x=L_{\mathrm{A}}}$$

$$= \mu_{\mathrm{nE}}F_{\mathrm{E}} \exp\left(\frac{-\mu_{\mathrm{nE}}F_{\mathrm{E}}L_{\mathrm{A}}}{D_{\mathrm{nE}}}\right) n_{\mathrm{E}}\big|_{x=L_{\mathrm{A}}+L_{\mathrm{E}}} \tag{72}$$

where $n_{\mathrm{E}}\big|_{x=L_{\mathrm{A}}+L_{\mathrm{E}}}$ is given by Eq. (65).

To obtain the boundary condition at $x = L_{\mathrm{A}}$ for Eq. (2), we start with the continuity equation for free holes in the ETL at steady state [which has a similar form to Eq. (2), but with zero carrier photogeneration rate and zero net nongeminate recombination rate as explained in Sect. 2.1], which is

$$-\frac{1}{q}\frac{\partial J_{\mathrm{pE}}}{\partial x} = D_{\mathrm{pE}}\frac{\partial^2 p_{\mathrm{E}}}{\partial x^2} - \mu_{\mathrm{pE}}F_{\mathrm{E}}\frac{\partial p_{\mathrm{E}}}{\partial x} = 0 \tag{73}$$

The general solution to Eq. (73) is

$$p_{\mathrm{E}} = A_7 \exp\left(\frac{\mu_{\mathrm{pE}}F_{\mathrm{E}}x}{D_{\mathrm{pE}}}\right) + A_8 \tag{74}$$

where A_7 and A_8 are constants that can be obtained by applying the boundary conditions, one at $x = L_{\mathrm{A}} + L_{\mathrm{E}}$ and another at $x = L_{\mathrm{A}}$. At $x = L_{\mathrm{A}} + L_{\mathrm{E}}$, the hole quasi-Fermi level must coincide with E_{Fc}, and thus by using the Boltzmann statistics, the boundary condition for Eq. (73) at $x = L_{\mathrm{A}} + L_{\mathrm{E}}$ is

$$p_{\mathrm{E}}\big|_{x=L_{\mathrm{A}}+L_{\mathrm{E}}} = N_{\mathrm{vE}} \exp\left[\frac{-\left(E_{\mathrm{Fc}} - \mathrm{HOMO_E}\right)}{k_{\mathrm{B}}T}\right] \tag{75}$$

where N_{vE} is the effective DoS in the valence band of the ETL. There must be a continuity in the hole quasi-Fermi level inside the device including at $x = L_{\mathrm{A}}$, and by using the same approach as in Sect. 2.3.3 [refer Eqs. (52) and (53)], it can be shown that the boundary condition for Eq. (73) at $x = L_{\mathrm{A}}$ is

$$p_{\mathrm{E}}\big|_{x=L_{\mathrm{A}}} = \alpha_4\, p_{\mathrm{A}}\big|_{x=L_{\mathrm{A}}} \tag{76}$$

where

$$\alpha_4 = \frac{N_{\mathrm{vE}}}{N_{\mathrm{vdA}}} \exp\left(\frac{\mathrm{HOMO_E} - \mathrm{HOMO_{dA}}}{k_{\mathrm{B}}T}\right) \tag{77}$$

Applying the two boundary conditions [i.e., Eqs. (75) and (76)] to the solution of Eq. (73) [i.e., Eq. (74)], we get

$$A_7 = \frac{p_{\mathrm{E}}\big|_{x=L_{\mathrm{A}}+L_{\mathrm{E}}} - p_{\mathrm{E}}\big|_{x=L_{\mathrm{A}}}}{\beta_4} \tag{78}$$

$$A_8 = \frac{p_{\mathrm{E}}\big|_{x=L_{\mathrm{A}}} \exp\left[\frac{\mu_{\mathrm{pE}}F_{\mathrm{E}}\left(L_{\mathrm{A}}+L_{\mathrm{E}}\right)}{D_{\mathrm{pE}}}\right] - p_{\mathrm{E}}\big|_{x=L_{\mathrm{A}}+L_{\mathrm{E}}} \exp\left(\frac{\mu_{\mathrm{pE}}F_{\mathrm{E}}L_{\mathrm{A}}}{D_{\mathrm{pE}}}\right)}{\beta_4} \tag{79}$$

with

$$\beta_4 = \exp\left[\frac{\mu_{pE}F_E(L_A+L_E)}{D_{pE}}\right] - \exp\left(\frac{\mu_{pE}F_E L_A}{D_{pE}}\right) \tag{80}$$

where $p_E|_{x=L_A+L_E}$ and $p_E|_{x=L_A}$ are given by Eqs. (75) and (76), respectively.

Furthermore, the hole current continuity at $x = L_A$ means that $J_{pE}\big|_{x=L_A} = J_{pA}\big|_{x=L_A}$ where J_{pE} and J_{pA} are given by Eqs. (62) and (4), respectively. Applying the hole current continuity at $x = L_A$ interface, we have

$$\mu_{pE}F_E p_E|_{x=L_A} - D_{pE}\frac{\partial p_E}{\partial x}\bigg|_{x=L_A} = \mu_{pA}F_A p_A|_{x=L_A} - D_{pA}\frac{\partial p_A}{\partial x}\bigg|_{x=L_A} \tag{81}$$

We can replace $(\partial p_E/\partial x)\big|_{x=L_A}$ and $p_E|_{x=L_A}$ in Eq. (81) with the derivative of Eq. (74) at $x = L_A$ and Eq. (76), respectively, to obtain the boundary condition at $x = L_A$ for Eq. (2), which is given by

$$\left(\mu_{pE}F_E\alpha_4 \exp\left[\frac{\mu_{pE}F_E(L_A+L_E)}{D_{pE}}\right] - \mu_{pA}F_A\beta_4\right)p_A|_{x=L_A} + \beta_4 D_{pA}\frac{\partial p_A}{\partial x}\bigg|_{x=L_A}$$

$$= \mu_{pE}F_E \exp\left(\frac{\mu_{pE}F_E L_A}{D_{pE}}\right)p_E|_{x=L_A+L_E} \tag{82}$$

where $p_E|_{x=L_A+L_E}$ is given by Eq. (75).

It is worth noting that F_A and F_E can be zero at a certain V_a (note that $F_A = F_E$ for the device in this case as explained in Sect. 2.2.1 or Sect. 2.2.3 for example). When F_A and F_E are zero, $\beta_3 = 0$ [see Eq. (70)] and thus A_5 and A_6 are undefined (the same happens with A_7 and A_8 because $\beta_4 = 0$ too). Nevertheless, when F_A and F_E are zero, Eqs. (72) and (82) can still be used for the device in this case, but by using values of F_A and F_E that are very close to zero, not exactly zero. Alternatively (and more accurately), when F_A and F_E are zero, the boundary conditions at $x = L_A$ for Eqs. (1) and (2) for the device in this case are the same as the boundary conditions at $x = L_A$ for Eqs. (1) and (2) for the device described in Sect. 2.3.6 (by applying $F_A = 0$ to the boundary conditions obtained in Sect. 2.3.6).

2.3.5 Boundary conditions at $x = 0$ for the device with the HTL made of a semiconductor with mobile carriers

For the device in this case, we assume the HTL is made of an inorganic semiconductor, and hence CBM_H and VBM_H are used here instead of $LUMO_H$ and $HOMO_H$. It is worth noting that it is possible for an organic semiconductor to have mobile carriers if it is doped [19]. Hence, if a doped organic semiconductor is used instead of an inorganic semiconductor, then CBM_H and VBM_H should be replaced with $LUMO_H$ and $HOMO_H$, respectively. The anode-HTL and the HTL-active layer interfaces are located at $x = -L_H$ and $x = 0$, respectively (see Fig. 1), and can be treated like metal–semiconductor and semiconductor-insulator contacts, respectively (see the explanation in Sect. 2.2.1). As explained in Sect. 2.2.4, we take the HTL to be a strong p-type material.

We can approximate $F_H = 0$ if the HTL is made of a semiconductor with mobile carriers because the semiconductor is a strong p-type material (see the explanation in Sect. 2.2.4). Furthermore, as mentioned in Sect. 2.1, we assume that the carrier mobilities, temperatures, and electric fields inside all layers to be uniform, and we also assume that the carrier photogeneration rate and the net nongeminate recombination rate in the HTL to be zero. Therefore, the continuity equation for electrons in the HTL at steady state is as given by Eq. (37) but with $F_H = 0$. The general solution to Eq. (37) with $F_H = 0$ is

$$n_H = A_9 x + A_{10} \tag{83}$$

where A_9 and A_{10} are constants that can be obtained by applying the boundary conditions, one at $x = -L_H$ and the other at $x = 0$.

For the case when $E_{FH} = E_{Fa}$, the Fermi level in the HTL at $x = -L_H$ is obviously given by E_{FH} (which obviously equals E_{Fa}). For the case when $E_{FH} \neq E_{Fa}$, the resulting depletion layer is negligibly thin (see the explanation in Sect. 2.2.4) such that the position $x = -L_H$ on the HTL side is approximately the same as the position of the edge of that thin depletion layer. Hence, the Fermi level at $x = -L_H$ on the HTL side for the case when $E_{FH} \neq E_{Fa}$ can be taken to be E_{FH} too (however, it is worth noting that the Fermi level at $x = -L_H$ on the anode side is given by E_{Fa}). Using the Boltzmann statistics, this means that whether E_{FH} equals E_{Fa} or not, the boundary condition at $x = -L_H$ for Eq. (83) can be taken to be

$$n_H|_{x=-L_H} = N_{cH}\exp\left[\frac{-(CBM_H - E_{FH})}{k_B T}\right] \tag{84}$$

There must be a continuity in the electron quasi-Fermi level inside the device including at $x = 0$, and by using the same approach as in Sect. 2.3.3 [refer Eqs. (40) and (41)], it can be shown that the boundary condition at $x = 0$ for Eq. (83) is given by

$$n_{\mathrm{H}}\big|_{x=0} = \alpha_5\, n_{\mathrm{A}}\big|_{x=0} \tag{85}$$

with

$$\alpha_5 = \frac{N_{\mathrm{cH}}}{N_{\mathrm{caA}}} \exp\left(\frac{\mathrm{LUMO_{aA}} - \mathrm{CBM_H}}{k_{\mathrm{B}}T}\right) \tag{86}$$

Applying the two boundary conditions [i.e., Eqs. (84) and (85)] to Eq. (83), we get

$$A_9 = \frac{n_{\mathrm{H}}\big|_{x=0} - n_{\mathrm{H}}\big|_{x=-L_{\mathrm{H}}}}{L_{\mathrm{H}}} \tag{87}$$

$$A_{10} = n_{\mathrm{H}}\big|_{x=0} \tag{88}$$

where $n_{\mathrm{H}}\big|_{x=-L_{\mathrm{H}}}$ and $n_{\mathrm{H}}\big|_{x=0}$ are given by Eqs. (84) and (85), respectively.

Furthermore, the electron current continuity at $x = 0$ means that $J_{\mathrm{nH}}\big|_{x=0} = J_{\mathrm{nA}}\big|_{x=0}$ where J_{nH} and J_{nA} are given by Eq. (35) with $F_{\mathrm{H}} = 0$ and Eq. (3), respectively. Applying the electron current continuity at $x = 0$ interface, we have

$$D_{\mathrm{nH}} \left.\frac{\partial n_{\mathrm{H}}}{\partial x}\right|_{x=0} = \mu_{\mathrm{nA}} F_{\mathrm{A}}\, n_{\mathrm{A}}\big|_{x=0} + D_{\mathrm{nA}} \left.\frac{\partial n_{\mathrm{A}}}{\partial x}\right|_{x=0} \tag{89}$$

We can replace $\left(\partial n_{\mathrm{H}}/\partial x\right)\big|_{x=0}$ in Eq. (89) with the derivative of Eq. (83) at $x = 0$, and we can replace $n_{\mathrm{H}}\big|_{x=0}$ that appears in $\left(\partial n_{\mathrm{H}}/\partial x\right)\big|_{x=0}$ with Eq. (85), to obtain the boundary condition at $x = 0$ for Eq. (1), which is given by

$$\left(D_{\mathrm{nH}}\alpha_5 - \mu_{\mathrm{nA}} F_{\mathrm{A}} L_{\mathrm{H}}\right) n_{\mathrm{A}}\big|_{x=0} - D_{\mathrm{nA}} L_{\mathrm{H}} \left.\frac{\partial n_{\mathrm{A}}}{\partial x}\right|_{x=0} = D_{\mathrm{nH}}\, n_{\mathrm{H}}\big|_{x=-L_{\mathrm{H}}} \tag{90}$$

where $n_{\mathrm{H}}\big|_{x=-L_{\mathrm{H}}}$ is given by Eq. (84).

To obtain the boundary condition at $x = 0$ for Eq. (2), we start with the continuity equation for free holes in the HTL at steady state, which is given by Eq. (49) but with $F_{\mathrm{H}} = 0$ for the device in this case. The general solution to Eq. (49) with $F_{\mathrm{H}} = 0$ is

$$p_{\mathrm{H}} = A_{11}x + A_{12} \tag{91}$$

where A_{11} and A_{12} are constants that can be obtained by applying the boundary conditions, one at $x = -L_{\mathrm{H}}$ and another at $x = 0$.

As discussed above, the Fermi level in the HTL at $x = -L_{\mathrm{H}}$ can be taken to be E_{FH} whether E_{FH} equals E_{Fa} or not. Using the Boltzmann statistics, the boundary condition for Eq. (91) at $x = -L_{\mathrm{H}}$ whether E_{FH} equals E_{Fa} or not is given by

$$p_{\mathrm{H}}\big|_{x=-L_{\mathrm{H}}} = N_{\mathrm{vH}} \exp\left[\frac{-\left(E_{\mathrm{FH}} - \mathrm{VBM_H}\right)}{k_{\mathrm{B}}T}\right] \tag{92}$$

There must be a continuity in the hole quasi-Fermi level inside the device including at $x = 0$, and by using the same approach as in Sect. 2.3.3 [refer Eqs. (52) and (53)], it can be shown that the boundary condition at $x = 0$ for Eq. (91) is given by

$$p_{\mathrm{H}}\big|_{x=0} = \alpha_6\, p_{\mathrm{A}}\big|_{x=0} \tag{93}$$

with

$$\alpha_6 = \frac{N_{\mathrm{vH}}}{N_{\mathrm{vdA}}} \exp\left(\frac{\mathrm{VBM_H} - \mathrm{HOMO_{dA}}}{k_{\mathrm{B}}T}\right) \tag{94}$$

Applying the two boundary conditions [i.e., Eqs. (92) and (93)] to Eq. (91), we get

$$A_{11} = \frac{p_{\mathrm{H}}\big|_{x=0} - p_{\mathrm{H}}\big|_{x=-L_{\mathrm{H}}}}{L_{\mathrm{H}}} \tag{95}$$

$$A_{12} = p_{\mathrm{H}}\big|_{x=0} \tag{96}$$

where $p_{\mathrm{H}}\big|_{x=-L_{\mathrm{H}}}$ and $p_{\mathrm{H}}\big|_{x=0}$ are given by Eqs. (92) and (93), respectively.

Furthermore, the hole current continuity at $x = 0$ means that $J_{\mathrm{pH}}\big|_{x=0} = J_{\mathrm{pA}}\big|_{x=0}$ where J_{pH} and J_{pA} are given by Eq. (36) with $F_{\mathrm{H}} = 0$ and Eq. (4), respectively. Applying the hole current continuity at $x = 0$ interface, we have

$$-D_{\mathrm{pH}} \left.\frac{\partial p_{\mathrm{H}}}{\partial x}\right|_{x=0} = \mu_{\mathrm{pA}} F_{\mathrm{A}}\, p_{\mathrm{A}}\big|_{x=0} - D_{\mathrm{pA}} \left.\frac{\partial p_{\mathrm{A}}}{\partial x}\right|_{x=0} \tag{97}$$

We can replace $\left(\partial p_{\mathrm{H}}/\partial x\right)\big|_{x=0}$ in Eq. (97) with the derivative of Eq. (91) at $x = 0$, and we can replace $p_{\mathrm{H}}\big|_{x=0}$ that appears in $\left(\partial p_{\mathrm{H}}/\partial x\right)\big|_{x=0}$ with Eq. (93), to obtain the boundary condition at $x = 0$ for Eq. (2), which is given by

$$\left(\alpha_6 D_{\mathrm{pH}} + \mu_{\mathrm{pA}} F_{\mathrm{A}} L_{\mathrm{H}}\right) p_{\mathrm{A}}\big|_{x=0} - D_{\mathrm{pA}} L_{\mathrm{H}} \left.\frac{\partial p_{\mathrm{A}}}{\partial x}\right|_{x=0} = D_{\mathrm{pH}}\, p_{\mathrm{H}}\big|_{x=-L_{\mathrm{H}}} \tag{98}$$

where $p_{\mathrm{H}}\big|_{x=-L_{\mathrm{H}}}$ is given by Eq. (92).

2.3.6 Boundary conditions at $x = L_{\mathrm{A}}$ for the device with the ETL made of a semiconductor with mobile carriers

For the device in this case, we assume the ETL is made of an inorganic semiconductor, and hence $\mathrm{CBM_E}$ and $\mathrm{VBM_E}$ are used here instead of $\mathrm{LUMO_E}$ and $\mathrm{HOMO_E}$. The active layer-ETL and the ETL-cathode interfaces are located at $x = L_{\mathrm{A}}$ and $x = L_{\mathrm{A}} + L_{\mathrm{E}}$, respectively (see Fig. 1), and can be treated like insulator-semiconductor and semiconductor–metal contacts, respectively (see the explanation in Sect. 2.2.1). As explained in Sect. 2.2.4, we take the ETL to be a strong n-type material.

We can approximate $F_E = 0$ if the ETL is made of a semiconductor with mobile carriers because the semiconductor is a strong n-type material (see the explanation in Sect. 2.2.4). Furthermore, as mentioned in Sect. 2.1, we assume that the carrier mobilities, temperatures, and electric fields inside all layers to be uniform, and we also assume that the carrier photogeneration rate and the net nongeminate recombination rate in the ETL to be zero. Therefore, the continuity equation for electrons in the ETL at steady state is as given by Eq. (63) but with $F_E = 0$. The general solution to Eq. (63) with $F_E = 0$ is

$$n_E = A_{13}x + A_{14} \tag{99}$$

where A_{13} and A_{14} are constants that can be obtained by applying the boundary conditions, one at $x = L_A + L_E$ and the other at $x = L_A$.

For the case when $E_{FE} = E_{Fc}$, the Fermi level in the ETL at $x = L_A + L_E$ is obviously given by E_{FE} (which obviously equals E_{Fc}). For the case when $E_{FE} \neq E_{Fc}$, the resulting depletion layer is negligibly thin (see the explanation in Sect. 2.2.4) such that the position $x = L_A + L_E$ on the ETL side is approximately the same as the position of the edge of that thin depletion layer. Hence, the Fermi level at $x = L_A + L_E$ on the ETL side for the case when $E_{FE} \neq E_{Fc}$ can be taken to be E_{FE} too (however, it is worth noting that the Fermi level at $x = L_A + L_E$ on the cathode side is given by E_{Fc}). Using the Boltzmann statistics, this means that whether E_{FE} equals E_{Fc} or not, the boundary condition at $x = L_A + L_E$ for Eq. (99) can be taken to be

$$n_E\big|_{x=L_A+L_E} = N_{cE} \exp\left[\frac{-(\mathrm{CBM}_E - E_{FE})}{k_B T}\right] \tag{100}$$

There must be a continuity in the electron quasi-Fermi level inside the device including at $x = L_A$, and by using the same approach as in Sect. 2.3.3 [refer Eqs. (40) and (41)], it can be shown that the boundary condition at $x = L_A$ for Eq. (99) is given by

$$n_E\big|_{x=L_A} = \alpha_7\, n_A\big|_{x=L_A} \tag{101}$$

with

$$\alpha_7 = \frac{N_{cE}}{N_{caA}} \exp\left(\frac{\mathrm{LUMO}_{aA} - \mathrm{CBM}_E}{k_B T}\right) \tag{102}$$

Applying the two boundary conditions [i.e., Eqs. (100) and (101)] to Eq. (99), we get

$$A_{13} = \frac{n_E\big|_{x=L_A+L_E} - n_E\big|_{x=L_A}}{L_E} \tag{103}$$

$$A_{14} = \frac{(L_A + L_E) n_E\big|_{x=L_A} - L_A\, n_E\big|_{x=L_A+L_E}}{L_E} \tag{104}$$

where $n_E\big|_{x=L_A+L_E}$ and $n_E\big|_{x=L_A}$ are given by Eqs. (100) and (101), respectively.

Moreover, the electron current continuity at $x = L_A$ means that $J_{nE}\big|_{x=L_A} = J_{nA}\big|_{x=L_A}$ where J_{nE} and J_{nA} are given by Eq. (61) with $F_E = 0$ and Eq. (3), respectively. Applying the electron current continuity at $x = L_A$ interface, we have

$$D_{nE} \left.\frac{\partial n_E}{\partial x}\right|_{x=L_A} = \mu_{nA} F_A\, n_A\big|_{x=L_A} + D_{nA} \left.\frac{\partial n_A}{\partial x}\right|_{x=L_A} \tag{105}$$

We can replace $\left(\partial n_E / \partial x\right)\big|_{x=L_A}$ in Eq. (105) with the derivative of Eq. (99) at $x = L_A$, and we can replace $n_E\big|_{x=L_A}$ that appears in $\left(\partial n_E / \partial x\right)\big|_{x=L_A}$ with Eq. (101), to obtain the boundary condition at $x = L_A$ for Eq. (1), which is given by

$$\left(D_{nE}\alpha_7 + \mu_{nA} F_A L_E\right) n_A\big|_{x=L_A} + D_{nA} L_E \left.\frac{\partial n_A}{\partial x}\right|_{x=L_A} = D_{nE}\, n_E\big|_{x=L_A+L_E} \tag{106}$$

where $n_E\big|_{x=L_A+L_E}$ is given by Eq. (100).

To obtain the boundary condition at $x = L_A$ for Eq. (2), we start with the continuity equation for free holes in the ETL at steady state, which is given by Eq. (73) but with $F_E = 0$ for the device in this case. The general solution to Eq. (73) with $F_E = 0$ is

$$p_E = A_{15}x + A_{16} \tag{107}$$

where A_{15} and A_{16} are constants that can be obtained by applying the boundary conditions, one at $x = L_A + L_E$ and the other at $x = L_A$.

As discussed above, the Fermi level in the ETL at $x = L_A + L_E$ can be taken to be E_{FE} whether E_{FE} equals E_{Fc} or not. Using the Boltzmann statistics, the boundary condition for Eq. (107) at $x = L_A + L_E$ whether E_{FE} equals E_{Fc} or not is given by

$$p_E\big|_{x=L_A+L_E} = N_{vE} \exp\left[\frac{-(E_{FE} - \mathrm{VBM}_E)}{k_B T}\right] \tag{108}$$

There must be a continuity in the hole quasi-Fermi level inside the device including at $x = L_A$, and by using the same approach as in Sect. 2.3.3 [refer Eqs. (52) and (53)], it can be shown that the boundary condition at $x = L_A$ for Eq. (107) is given by

$$p_E\big|_{x=L_A} = \alpha_8\, p_A\big|_{x=L_A} \tag{109}$$

with

$$\alpha_8 = \frac{N_{vE}}{N_{vdA}} \exp\left(\frac{VBM_E - HOMO_{dA}}{k_B T}\right) \tag{110}$$

Applying the two boundary conditions [i.e., Eqs. (108) and (109)] to Eq. (107), we get

$$A_{15} = \frac{p_E\big|_{x=L_A+L_E} - p_E\big|_{x=L_A}}{L_E} \tag{111}$$

$$A_{16} = \frac{(L_A + L_E)p_E\Big|_{x=L_A} - L_A p_E\big|_{x=L_A+L_E}}{L_E} \tag{112}$$

where $p_E\big|_{x=L_A+L_E}$ and $p_E\big|_{x=L_A}$ are given by Eqs. (108) and (109), respectively.

Furthermore, the hole current continuity at $x = L_A$ means that $J_{pE}\Big|_{x=L_A} = J_{pA}\Big|_{x=L_A}$ where J_{pE} and J_{pA} are given by Eq. (62) with $F_E = 0$ and Eq. (4), respectively. Applying the hole current continuity at $x = L_A$ interface, we have

$$-D_{pE}\frac{\partial p_E}{\partial x}\bigg|_{x=L_A} = \mu_{pA}F_A p_A\big|_{x=L_A} - D_{pA}\frac{\partial p_A}{\partial x}\bigg|_{x=L_A} \tag{113}$$

We can replace $(\partial p_E/\partial x)\big|_{x=L_A}$ in Eq. (113) with the derivative of Eq. (107) at $x = L_A$, and we can replace $p_E\big|_{x=L_A}$ that appears in $(\partial p_E/\partial x)\big|_{x=L_A}$ with Eq. (109), to obtain the boundary condition at $x = L_A$ for Eq. (2), which is given by

$$(\alpha_8 D_{pE} - \mu_{pA}F_A L_E)\, p_A\big|_{x=L_A} + D_{pA}L_E\frac{\partial p_A}{\partial x}\bigg|_{x=L_A} = D_{pE}p_E\big|_{x=L_A+L_E} \tag{114}$$

where $p_E\big|_{x=L_A+L_E}$ is given by Eq. (108).

2.4 Obtaining the J-V characteristics

In order to calculate the nongeminate recombination rates and the current densities, we use the method proposed in Ref. [11], which can be described as follows. First, we solve the continuity equation for electrons (holes) in the active layer without considering the nongeminate recombination to obtain what we call the maximum electron (hole) concentration in the active layer $n_{A,max}$ ($p_{A,max}$). The method in Ref. [11] views $n_{A,max}$ ($p_{A,max}$) as the electron (hole) concentration inside the active layer that is available to participate in the nongeminate recombination. Hence, $n_{A,max}$ and $p_{A,max}$ are used for calculating the nongeminate recombination rates. Then, we solve the continuity equation for electrons (holes) in the active layer by including the nongeminate recombination rates attained earlier to obtain what we call the net electron (hole) concentration in the active layer $n_{A,net}$ ($p_{A,net}$). The method in Ref. [11] views $n_{A,net}$ ($p_{A,net}$) as the electron (hole) concentration inside the active layer that is available to generate the electron (hole) current density. Therefore, the obtained $n_{A,net}$ and $p_{A,net}$ are used for calculating J_{nA} and J_{pA}, respectively, which in turn enable us to obtain the total current density J, and hence the J-V characteristic.

The continuity equations for electrons and holes in the active layer [refer Eqs. (1) and (2)] at steady state without considering the nongeminate recombination are given by

$$D_{nA}\frac{\partial^2 n_{A,max}}{\partial x^2} + \mu_{nA}F_A\frac{\partial n_{A,max}}{\partial x} + P_d G_{CT} = 0 \tag{115}$$

$$D_{pA}\frac{\partial^2 p_{A,max}}{\partial x^2} - \mu_{pA}F_A\frac{\partial p_{A,max}}{\partial x} + P_d G_{CT} = 0 \tag{116}$$

where $n_{A,max}$ and $p_{A,max}$ are as defined above. F_A and the boundary conditions are as given in Sect. 2.2 and Sect. 2.3, respectively, depending on the device setting. To obtain analytical expressions for $n_{A,max}$ and $p_{A,max}$, we need to analytically solve Eqs. (115) and (116), respectively. To achieve this, the combined analytical and regression method proposed in Ref. [8] is used to solve Eqs. (115) and (116) and obtain analytical expressions for $n_{A,max}$ and $p_{A,max}$.

As mentioned earlier in this section, the obtained $n_{A,max}$ and $p_{A,max}$ are used to calculate the nongeminate recombination rates in the active layer. Therefore, the bimolecular recombination rate per unit volume R_b is given by [8, 12]

$$R_b = \gamma k_L\left(n_{A,max}p_{A,max} - n_0 p_0\right) \tag{117}$$

where γ is the bimolecular recombination reduction coefficient, and $k_L = q\left(\mu_{nA} + \mu_{pA}\right)/\varepsilon_A$ is the Langevin recombination coefficient with ε_A being the effective permittivity of the active layer. Here, we use n_0 and p_0 as proposed in Ref. [12] where n_0 and p_0 are the solutions to $\partial J_{nA}/\partial x = 0$ and $\partial J_{pA}/\partial x = 0$, respectively (note that the applicable boundary conditions as given in Sect. 2.3 must be applied to solve $\partial J_{nA}/\partial x = 0$ and $\partial J_{pA}/\partial x = 0$). However, the conventional $n_0 p_0 = n_{int}^2$ where n_{int} is the intrinsic carrier concentration can also be used if wished. The trap-assisted recombination rate per unit volume R_{trap} is given by [8, 12]

$$R_{trap} = \frac{v_{th}\sigma_n\sigma_p N_{trap}\left(n_{A,max}p_{A,max} - n_0 p_0\right)}{\sigma_n\left(n_{A,max} + n_1\right) + \sigma_p\left(p_{A,max} + p_1\right)} \tag{118}$$

where v_{th} is the electron thermal velocity, σ_n is the electron capture cross section, σ_p is the hole capture cross section, N_{trap} is the trap density, and n_1 and p_1 are given by

$$n_1 = N_{caA}\exp\left(\frac{E_{trap} - LUMO_{aA}}{k_B T}\right) \tag{119}$$

$$p_1 = N_{vdA}\exp\left(\frac{HOMO_{dA} - E_{trap}}{k_B T}\right) \tag{120}$$

where E_{trap} is the trap energy level. The Auger recombination rate per unit volume R_A is given by [812]

$$R_A = \left(k_{A1} n_{A,max} + k_{A2} p_{A,max}\right)\left(n_{A,max} p_{A,max} - n_0 p_0\right) \quad (121)$$

where k_{A1} and k_{A2} are the Auger recombination coefficients.

The continuity equations for electrons and holes inside the active layer at steady state with the nongeminate recombination included [refer Eqs. (1) and (2)] are given by

$$D_{nA}\frac{\partial^2 n_{A,net}}{\partial x^2} + \mu_{nA} F_A \frac{\partial n_{A,net}}{\partial x} + P_d\left(G_{CT} + R_b\right) - \left(R_b + R_{trap} + R_A\right) = 0 \quad (122)$$

$$D_{pA}\frac{\partial^2 p_{A,net}}{\partial x^2} - \mu_{pA} F_A \frac{\partial p_{A,net}}{\partial x} + P_d\left(G_{CT} + R_b\right) - \left(R_b + R_{trap} + R_A\right) = 0 \quad (123)$$

where $n_{A,net}$ and $p_{A,net}$ are as defined earlier in this Sect. 2.4 , while F_A (see Sect. 2.2) and the boundary conditions (see Sect. 2.3) depend on the device setting. To obtain analytical expressions for $n_{A,net}$ and $p_{A,net}$, Eqs. (122) and (123) need to be analytically solved. Again, the same as for Eqs. (115) and (116), the method proposed in Ref. [8] is used to solve Eqs. (122) and (123) in order to obtain analytical expressions for $n_{A,net}$ and $p_{A,net}$.

As described earlier in this Sect. 2.4, the obtained $n_{A,net}$ and $p_{A,net}$ are then used to calculate J_{nA} and J_{pA}, which are given by

$$J_{nA} = q\mu_{nA} F_A n_{A,net} + qD_{nA}\frac{\partial n_{A,net}}{\partial x} \quad (124)$$

$$J_{pA} = q\mu_{pA} F_A p_{A,net} - qD_{pA}\frac{\partial p_{A,net}}{\partial x} \quad (125)$$

The total current density J is given by

$$J = J_{nA} + J_{pA} \quad (126)$$

where J is uniform and can be obtained by adding the values of J_{nA} and J_{pA} evaluated at any given position within the active layer.

It is worth mentioning again that the use of the combined analytical and regression method [8] would make the proposed drift–diffusion-based J-V model to be more accurate than analytical drift–diffusion-based J-V models and more reliable than numerical drift–diffusion-based J-V models.

3 Results and discussion

In practice, the inclusion of CTLs affects (preferably improve) the PCE of OSCs through several ways. For example, the inclusion of CTLs can affect the charge carrier extraction or collection by the electrodes by blocking the unwanted carrier types but still allowing the desired carrier types to be efficiently extracted (provided that the CTLs are not too thick because thick CTLs could make the extraction of the desired carrier types to be significantly less efficient). The proposed J-V model can evaluate and predict how the inclusion of CTLs affects the charge carrier extraction, and consequently, how the charge carrier extraction affects the J-V characteristic, and thus the PCE.

Furthermore, the inclusion of CTLs should also decrease the loss of excitons by blocking the photogenerated excitons, particularly near the edges of the active layer, from diffusing to the electrodes. This means more excitons can become CT states (thus increasing G_{CT}) and then free charge carriers. Therefore, after the inclusion of CTLs, an OSC could have a higher G_{CT}, and hence a higher PCE. To take account of the decrease in the loss of excitons, all that we can do is to use a higher G_{CT} value in the proposed J-V model. However, how much the value of G_{CT} should increase after the inclusion of CTLs cannot be evaluated and predicted by the proposed J-V model (since an optical modeling is currently not included with the proposed J-V model). Similarly, the proposed J-V model also cannot evaluate and predict how N_{trap}, particularly at the active layer-CTL interfaces, would change if CTLs are added to an OSC (of course N_{trap} affects the carrier recombination and thus the PCE). To validate the proposed J-V model, ideally, we should show that the model can satisfactorily fit the experimental J-V characteristics of OSCs both before (without) and after (with) the inclusion of CTLs. However, it would be challenging and could be impractical trying to validate the proposed J-V model using this approach because as explained above, the proposed J-V model cannot evaluate and predict how the inclusion of CTLs affects some of the performance influencing factors such as G_{CT} and N_{trap} (i.e., we cannot predict and know what are the correct changes in the values of G_{CT} and N_{trap} that should be used after the inclusion of CTLs).

To validate any given model, we basically need to demonstrate that the model is able to do what it is designed to do. It is widely known that if a CTL with suitable properties (e.g., suitable energy levels, conductivity, and thickness) is added to an OSC, the PCE should improve because of the improvement in the charge carrier extraction (of course provided that the other performance influencing factors such as G_{CT} and N_{trap} are at least unchanged, if not

become better, after the CTL is added). Therefore, if we can show that the proposed J-V model predicts that the inclusion of a suitable CTL improves the PCE of an OSC because it improves the charge carrier extraction (with the other performance influencing factors assumed to be unchanged), then this demonstrates that the model works as it is designed to, and this can also serve as an alternative validation method.

Hence, to validate the proposed J-V model, we compare between the J-V characteristic of an OSC without CTLs (device A), the J-V characteristic of an OSC with the ETL made of a semiconductor with mobile carriers (device B), and the J-V characteristic of an OSC with the ETL made of a semiconductor without mobile carriers (device C), where the J-V characteristics are calculated using the J-V model proposed in this paper. We assume that all device properties remain unchanged after the ETL is included. We also choose $E_{Fc} = E_{FE}$ so that the built-in voltages across device A, device B, and device C are the same for a fair comparison between the devices. Table 2 shows the parameter values used in all calculations unless otherwise specified. The parameter values in Table 2 are typical for OSCs as used in our previous works [8, 11], whereas the values for N_{trap}, σ_n, and σ_p are the same as in Ref. [20] (note that Ref. [20] combined the electron and the hole capture cross sections with the carrier thermal velocity). MATLAB is used for all calculations including for solving Eqs. (115), (116), (122), and (123). If the PCEs of device B and device C are better than the PCE of device A, then this suggests that the proposed J-V model works well because we employ ETLs with the right properties in device B and device C.

Figure 2 shows the J-V characteristics of device A, device B, and device C. Assuming that the incident light intensity is 1000 Wm^{-2}, the PCEs of device A, device B, and device C are 6.86%, 7.38%, and 7.31%, respectively. Therefore, the results suggest that the proposed J-V model works well. To reveal the reason behind the increase in the PCE when an ETL is added, we calculate the electron and the hole current densities at $x = L_A$ at short circuit ($V_a = 0$) for all devices, which are shown in Table 3. As expected, Table 3 shows that although the inclusion of an ETL decreases the extraction of the desired carrier type (i.e., electrons) toward the cathode, but it decreases the extraction of the unwanted carrier type (i.e., holes) toward the cathode even more, and this increases the PCE overall. This also demonstrates that the proposed J-V model can reveal important insights into how and how much the performance of OSCs with CTLs can be improved, at least via the charge carrier extraction. It is worth mentioning that if a suitable HTL is also added (in addition to the ETL) to device B and device C, the PCEs of device B and device C are expected to be even higher.

To further demonstrate the applicability of the proposed model, we repeat the calculations by changing the thickness of the ETLs in device B and device C to 100 nm, while the other properties remain the same as in Table 2. By changing L_E from 40 to 100 nm, device B records a very small reduction in the PCE (a reduction of 0.0015% in the PCE), while device C records a significant reduction in the PCE (the PCE is reduced from 7.31% to 6.70%, which is now lower than the PCE of device A). It should be noted that in reality, there are factors that are not considered in the proposed model

Table 2 Parameter values used in all calculations unless otherwise specified. Refer Table 1 for the description of the symbols

Symbol	Value
General device properties	
E_{Fa}	-4.9 eV
E_{Fc}	-4.0 eV
T	300 K
Active layer properties	
$LUMO_{aA}$	-3.8 eV
$HOMO_{dA}$	-5.1 eV
N_{caA}	2×10^{26} m^{-3}
N_{vdA}	2×10^{26} m^{-3}
μ_{nA}	1.8×10^{-7} m^2V^{-1} s^{-1}
$\mu_{nA,act}$	$200\mu_{n,A}$
μ_{pA}	2.8×10^{-8} m^2V^{-1} s^{-1}
$\mu_{pA,act}$	$200\mu_{p,A}$
k_f	1×10^{8} s^{-1}
a	1.8 nm
ε_A	3×10^{-11} F m^{-3}
λ	0.2
L_A	150 nm
G_{CT}	6.5×10^{27} m^{-3} s^{-1}
γ	0.1
v_{th}	1×10^{5} $m{\cdot}s^{-1}$
σ_n	2×10^{-23} m^2
σ_p	2×10^{-23} m^2
N_{trap}	5×10^{22} m^{-3}
E_{trap}	0.6 eV below $LUMO_{aA}$
General ETL properties	
L_E	40 nm
$LUMO_E$ or CBM_E	-3.8 eV
$HOMO_E$ or VBM_E	-6.0 eV
N_{cE}	2×10^{26} m^{-3}
N_{vE}	2×10^{26} m^{-3}
ETL properties (for ETL made of a semiconductor with mobile carriers)	
μ_{nE}	1.0×10^{-4} m^2V^{-1} s^{-1}
μ_{pE}	1.0×10^{-5} m^2V^{-1} s^{-1}
E_{FE}	-4.0 eV
ETL properties (for ETL made of a semiconductor without mobile carriers)	
μ_{nE}	1.0×10^{-7} m^2V^{-1} s^{-1}
μ_{pE}	1.0×10^{-8} m^2V^{-1} s^{-1}

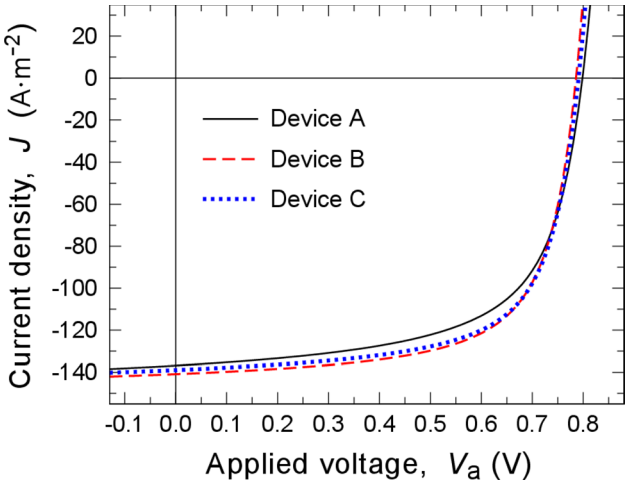

Fig. 2 The J-V characteristics of device A (no HTL and no ETL), device B (no HTL but with an ETL made of a semiconductor with mobile carriers), and device C (no HTL but with an ETL made of a semiconductor without mobile carriers) calculated using the proposed J-V model

Table 3 Electron current density in the active layer J_{nA} and hole current density in the active layer J_{pA} at $x = L_A$ at short circuit

Device	J_{nA}	J_{pA}
Device A	-141 A m^{-2}	4.17 A m^{-2}
Device B	-140.9 A m^{-2}	1.2×10^{-13} A m^{-2}
Device C	-139 A m^{-2}	-8.6×10^{-16} A m^{-2}

that can affect the PCE when the thickness of the CTL is changed. For example, a CTL actually absorbs some light (although ideally a CTL should not absorb light), and therefore, increasing the thickness of the CTL may increase the light absorption by the CTL, and hence may reduce the light absorption by the active layer, and thus may reduce the PCE too. Furthermore, as explained in Sect. 2.2.4, we assume that the ETL in device B to be an ideal conductor which leads to $F_E = 0$, but in reality, F_E for device B (where the ETL is made of a strong n-type semiconductor) is not zero (although relatively very small) and its value changes with V_a and is reduced when L_E is increased. Therefore, in reality, the PCE of device B should decrease by more than 0.0015% when L_E is increased from 40 to 100 nm. Nevertheless, the calculations here can still provide useful insights, for example by suggesting that semiconductors with mobile carriers are better candidates than semiconductors without mobile carriers in creating thickness-independent CTLs. Another conclusion that can be made from these calculations is that the thickness of CTLs should be kept as thin as possible if feasible, especially when semiconductors without mobile carriers are used as the CTLs.

It is worth mentioning that the model proposed here can also be extended to perovskite solar cells (PSCs). In PSCs, the active layer is typically made of an intrinsic perovskite material and both the HTL and ETL are always included in the device architecture. Since free carriers are directly generated upon light absorption in PSCs, G_n and G_p are not given by Eq. (8) anymore, but they are input parameters that directly depend on the light absorption by the active layer. Furthermore, in PSCs, the band-to-band recombination (the recombination between free electrons in the conduction band and free holes in the valence band of the perovskite material) replaces the bimolecular recombination.

4 Conclusions

In summary, we propose a model for describing the J-V characteristics of OSCs with CTLs. The model is based on the drift–diffusion transport model, which is the standard physics-based model for describing the transport of carriers in semiconductors. In obtaining the model, we derive the approximate electric fields and the approximate boundary conditions in OSCs with CTLs. The derived electric fields and boundary conditions are then applied to the carrier continuity equations, which are then solved using a recently proposed combined analytical and regression method [8] to obtain the J-V characteristics. The use of the method of Ref. [8] makes the proposed J-V model to be more accurate than analytical drift–diffusion-based J-V models (since the resulting model allows us to consider realistic carrier generation profiles and recombination mechanisms, which cannot be considered in analytical J-V models) and more reliable than numerical drift–diffusion-based J-V models (e.g., models based on finite difference method) [8]. We use the proposed model to calculate and compare between the J-V characteristics of an OSC without CTLs, an OSC with the ETL made of a semiconductor with mobile carriers, and an OSC with the ETL made of a semiconductor without mobile carriers. The results suggest that the proposed J-V model works well as it is designed to. We show that if a suitable CTL is used, the decrease in the extraction of the unwanted carrier type outweighs the decrease in the extraction of the desired carrier type, and this increases the PCE overall. Furthermore, we show that semiconductors with mobile carriers are better candidates than semiconductors without mobile carriers in creating thickness-independent CTLs, and the thickness of CTLs made of semiconductors without mobile carriers should be kept as thin as possible in order to maximize the PCE. These basically show that the proposed J-V model can be used to give valuable insights into how the PCE and the design (to reduce the cost for example) of OSCs with CTLs can be improved, particularly by optimizing the charge carrier extraction. Therefore, owing to its unique quality, the

proposed J-V model can be a valuable tool for predicting and improving the PCE, and optimizing the design of OSCs with CTLs. It is worth reminding that the proposed J-V model may not be able to accurately predict the J-V characteristics of OSCs with CTLs made of semiconductors with mobile carriers if the HTL and ETL are not made of a strong p-type and a strong n-type semiconductor, respectively. In the future, an optical modeling that describes the light absorption in OSCs can be incorporated in conjunction with the proposed J-V model in order to better predict how the PCE and the design of OSCs can be improved.

Acknowledgements The author acknowledges the support from the Fundamental Research Grant Scheme (FRGS/1/2017/STG02/UIAM/03/2).

Author Contribution All work presented in this article was performed by the sole author of this article.

Funding Open access funding provided by The Ministry of Higher Education Malaysia and International Islamic University Malaysia. The author would like to thank the Ministry of Higher Education of Malaysia for the grant (FRGS/1/2017/STG02/UIAM/03/2) and the Konsortium Sumber Elektronik Pendidikan Tinggi (KONSEPt) for the open access funding.

Data availability No datasets were generated or analysed during the current study.

Declarations

Conflict of interest The author declares no competing interests.

References

1. Seri, M., Mercuri, F., Ruani, G., Feng, Y., Li, M., Xu, Z., Muccini, M.: Toward real setting applications of organic and perovskite solar cells: a comparative review. Energy Technol. **9**, 2000901 (2001). https://doi.org/10.1002/ente.202000901
2. Chen, F.C.: Emerging organic and organic/inorganic hybrid photovoltaic devices for specialty applications: low-level-lighting energy conversion and biomedical treatment. Adv. Opt. Mater. **7**, 1800662 (2019). https://doi.org/10.1002/adom.201800662
3. O'Connor, T., Zaretski, A., Savagatrup, S., Printz, A., Wilkes, C., Diaz, M., Sawyer, E., Lipomi, D.: Wearable organic solar cells with high cyclic bending stability: materials selection criteria. Sol. Energy Mater. Sol. Cells **144**, 438 (2016). https://doi.org/10.1016/j.solmat.2015.09.049
4. Cui, Y., Wang, Y., Bergqvist, J., Yao, H., Xu, Y., Gao, B., Yang, C., Zhang, S., Inganas, O., Gao, F., Hou, J.: Wide-gap non-fullerene acceptor enabling high-performance organic photovoltaic cells for indoor applications. Nat. Energy **4**, 768 (2019). https://doi.org/10.1038/s41560-019-0448-5
5. Park, S., Heo, S.W., Lee, W., Inoue, D., Jiang, Z., Yu, K., Jinno, H., Hashizume, D., Sekino, M., Yokota, T., Fukuda, K., Tajima, K., Someya, T.: Self-powered ultra-flexible electronics via nano-grating-patterned organic photovoltaics. Nature **561**, 516 (2018). https://doi.org/10.1038/s41586-018-0536-x
6. NREL Best Research-Cell Efficiency Chart, https://www.nrel.gov/pv/cell-efficiency.html. Accessed 18 November 2024
7. Ouyang, D., Huang, Z., Choy, W.C.H.: Solution-processed metal oxide nanocrystals as carrier transport layers in organic and perovskite solar cells. Adv. Funct. Mater. **29**, 1804660 (2018). https://doi.org/10.1002/adfm.201804660
8. Inche Ibrahim, M.L.: A physics-based current-voltage model for organic solar cells using a combined analytical and regression approach. Appl. Phys. A **129**, 395 (2023). https://doi.org/10.1007/s00339-023-06645-7
9. Heeger, A.J.: 25th anniversary article: bulk heterojunction solar cells: Understanding the mechanism of operation. Adv. Mater. **26**, 10 (2014). https://doi.org/10.1002/adma.201304373
10. Proctor, C.M., Kuik, M., Nguyen, T.Q.: Charge carrier recombination in organic solar cells. Prog. Polym. Sci. **38**, 1941 (2013). https://doi.org/10.1016/j.progpolymsci.2013.08.008
11. Inche Ibrahim, M.L.: An analytical model for organic solar cells incorporating non-geminate monomolecular and bimolecular recombinations. Semicond. Sci. Technol. **33**, 125005 (2018). https://doi.org/10.1088/1361-6641/aadf72
12. Inche Ibrahim, M.L., Zakhidov, A.A.: An improved model for describing the net carrier recombination rate in semiconductor devices. Appl. Phys. A **128**, 21 (2022). https://doi.org/10.1007/s00339-021-05104-5
13. Braun, C.L.: Electric field assisted dissociation of charge transfer states as a mechanism of photocarrier production. J. Chem. Phys. **80**, 4157 (1984). https://doi.org/10.1063/1.447243
14. Inche Ibrahim, M.L.: Dissociation of charge-transfer states at donor–acceptor interfaces of organic heterojunctions. J. Phys. D Appl. Phys. **50**, 065103 (2017). https://doi.org/10.1088/1361-6463/50/6/065103
15. Riederer, P., Kersting, R.: Terahertz electromodulation spectroscopy for characterizing electronic transport in organic semiconductor thin films. J. Infrared Millim. Terahertz Waves **44**, 1 (2023). https://doi.org/10.1007/s10762-022-00893-z
16. Bisquert, J., Garcia-Belmonte, G.: On voltage, photovoltage, and photocurrent in bulk heterojunction organic solar cells. J. Phys. Chem. Lett. **2**, 1950 (2011). https://doi.org/10.1021/jz2004864
17. Brabec, C.J., Sariciftci, N.S., Hummelen, J.C.: Plastic solar cells. Adv. Funct. Mater. **11**, 15 (2001)
18. Hu, C.: Modern semiconductor devices for integrated circuits. Pearson/Prentice Hall, Upper Saddle River, New Jersey (2010) p. 96
19. Scaccabarozzi, A.D., Basu, A., Anies, F., Liu, J., Zapata-Arteaga, O., Warren, R., Firdaus, Y., Nugraha, M.I., Lin, Y., Campoy-Quiles, M., Koch, N., Muller, C., Tsetseris, L., Heeney, M., Anthopoulos, T.D.: Doping approaches for organic semiconductors. Chem. Rev. **122**, 4420 (2022). https://doi.org/10.1021/acs.chemrev.1c00581
20. Wetzelaer, G.A.H., Kuik, M., Nicolai, H.T., Blom, P.W.M.: Trap-assisted and Langevin-type recombination in organic light-emitting diodes. Phys. Rev. B **83**, 165204 (2011). https://doi.org/10.1103/PhysRevB.83.165204